STUDY OF HIGH-ENERGY GASES IMPINGING ON VARIOUS CRYOSURFACES

R. Dawbarn, M. R. Busby and M. Kinslow

ARO, Inc.

April 1972

VON KÁRMÁN GAS DYNAMICS FACILITY
ARNOLD ENGINEERING DEVELOPMENT CENTER
AIR FORCE SYSTEMS COMMAND
ARNOLD AIR FORCE STATION, TENNESSEE

NOTICES

When U. S. Government drawings specifications, or other data are used for any purpose other than a definitely related Government procurement operation, the Government thereby incurs no responsibility nor any obligation whatsoever, and the fact that the Government may have formulated, furnished, or in any way supplied the said drawings, specifications, or other data, is not to be regarded by implication or otherwise, or in any manner licensing the holder or any other person or corporation, or conveying any rights or permission to manufacture, use, or sell any patented invention that may in any way be related thereto.

Qualified users may obtain copies of this report from the Defense Documentation Center.

References to named commercial products in this report are not to be considered in any sense as an endorsement of the product by the United States Air Force or the Government.

STUDY OF HIGH-ENERGY GASES IMPINGING ON VARIOUS CRYOSURFACES

R. Dawbarn, M. R. Busby and M. Kinslow
ARO, Inc.

FOREWORD

The research reported herein was sponsored by the Arnold Engineering Development Center (AEDC), Air Force Systems Command (AFSC), Arnold Air Force Station, Tennessee, in support of Program Element 64719F.

The results of the research were obtained by ARO, Inc. (a subsidiary of Sverdrup & Parcel and Associates, Inc.), contract operator of the AEDC, AFSC, under Contract F40600-72-C-0003. The research was conducted from January 1970 to May 1971 under ARO Project VW3121. The manuscript was submitted for publication on January 14, 1972.

This technical report has been reviewed and is approved.

Michael G. Buja
Captain, USAF
Research and Development Division
Directorate of Technology

Robert O. Dietz
Acting Director
Directorate of Technology

ABSTRACT

A study of the interaction of high-energy molecular beams with various cryosurfaces was conducted in a molecular beam test facility. Spatial distributions of the reflected flux from several samples of typical engineering surfaces showed near-cosine distributions with some evidence of back scattering for roughened surfaces. For high-energy beams and highly polished surfaces there was a well-defined forward lobe of reflected molecules. Energy accommodation coefficients were determined by measuring the velocity of the reflected molecules. For all engineering surfaces tested the high-energy gases can be considered fully accommodated after one collision. Pumping studies of hydrogen (H_2) on liquid-helium (LHe)-cooled cryosurfaces were conducted. Capture coefficients close to 1.0 were measured for H_2 partial pressures up to 2×10^{-3} torr. For directed flows of H_2 on LHe-cooled panels there is an upper limit to the mass flow rate which will be cryopumped. This limit is determined by the thermal conductivity of the surface for stainless steel cryopanels and is apparently determined by cryofrost separation from the cryosurface for copper and aluminum cryopanels.

CONTENTS

APPENDIX
ILLUSTRATIONS

Figure

Figure | Page

NOMENCLATURE

c	Capture coefficient
E	Kinetic energy
k	Boltzmann constant
$\dot{n}$	Molecular flux, molecules/sec
p	Pressure, torr
Q	Gas flow rate, torr-liters/sec
S	Rate of strike, liters/sec
T	Temperature, °K
$\bar{v}$	Average velocity
α	Calibration factor for gage monitoring molecular beam
β	Ion gage calibration factor (torr/torr)
ϵ	Accommodation coefficient
θ	Angle with respect to surface normal
ξ	Fraction of mass flow incident on pump surface

SUBSCRIPTS AND SUPERSCRIPTS

77	Determined at 77°K
300	Determined at 300°K
a	Accommodated
g	Gage reading
i	Incident
o	Reservoir conditions
r	Reflected
s	Surface
t	Target
*	Directed flow

SECTION I
INTRODUCTION

The work reported herein is a part of a continuing effort to provide an improved capability for studying cryopumping of gases in a simulated space environment. One of the applications of cryopumping techniques previously developed has been in the production of a high-energy molecular beam by cryogenically skimming the core from a high temperature gas expanding from an aerodynamic nozzle (Refs. 1 and 2). A facility using this principle has been developed and provides a useful tool for studying in some detail the high temperature gas and cryosystem interaction.

The specific studies documented in this report were designed to determine the physical limitations in two areas of high-energy gas cryopumping: (1) precooling of hot gases, and (2) cryopumping of hydrogen (H_2). The first concerns the heat transfer between the incident high temperature gases and the pumping system. The basic concept of the high temperature gas cryopump involves the absorption of the bulk of the energy of the directed hot gas on a precooling surface and subsequent pumping of the reflected gas on cryosurfaces. In order to define the operating limits in such a system, it is necessary to know how much energy is transferred from the incident gas to the precooling surface and how the gas is reflected.

The studies discussed in Section II were conducted in the Aerodynamic Molecular Beam Chamber of the Aerospace Division, von Kármán Gas Dynamics Facility (VKF). The test gases were heated to temperatures typically found in a combustion process (2000 to 3000°K) and then expanded through a sonic orifice. A sample beam was then skimmed from the core of this expansion and used to investigate the high-energy gas and cryosurface interaction. The details of these experiments and the results are included in Section II of this report.

The second area of concern is focused on the cryopumping of H_2 on liquid-helium (LHe)-cooled surfaces. Available data in the literature (Ref. 3) and previous work conducted at AEDC-VKF (Ref. 4) indicate that the capture coefficient of H_2 on 4.2°K surfaces is between 0.9 and 1.0. However, these data were taken at pressures in the 10^{-5} to 10^{-10} torr range. In many tests H_2 partial pressure levels of 10^{-3} torr are experienced. Also, in some diagnostic probe applications, small LHe-cooled cryopumps are exposed to direct incidence of H_2 beams, where the molecular strike rates are well in excess of that from 10^{-3} torr ambient pressure levels. Additional problems in H_2 pumping on

LHe-cooled surfaces were discovered while trying to produce a high-energy H_2 beam in the molecular beam cell during the first phase of these studies. Poor frost adhesion, extreme sensitivity to radiation heat loads, and apparently a low capture coefficient all contributed to a marginal beam performance. Tests were therefore conducted in the 2- by 3-ft Research Vacuum Chamber to investigate the operation of LHe cryopumps at high chamber pressures and to note their behavior when exposed to gas loads from directed flows. The descriptions of these experiments and a discussion of the results are presented in Section III.

SECTION II
HIGH-ENERGY GAS AND CRYOSURFACE INTERACTION STUDIES

2.1 APPARATUS

2.1.1 Aerodynamic Molecular Beam Chamber

The AEDC-VKF Aerodynamic Molecular Beam experimental test cell (Fig. 1, Appendix) is a stainless steel cylinder, 3 ft in diameter by 6.5 ft in length, which is subdivided into three sections by bulkheads. The first bulkhead separates the source section of the cell from the collimation section and serves as a mounting base for the beam skimmer. The beam collimator is mounted on the second bulkhead which separates the collimation and test sections of the cell. The beam system and its performance are presented in detail in an unpublished report by Bailey, Busby, and Dawbarn of AEDC.

Vacuum conditions were produced and maintained in the source section by a 6-in. diffusion pump, a 20°K gaseous-helium (GHe) cryoliner, and a 77°K liquid-nitrogen (LN_2)-cooled cryoliner. Depending on the mass flow rate from the beam source, operating pressures from 10^{-4} to 10^{-7} torr were maintained in this section.

The aerodynamic molecular beam source (Fig. 2) was mounted in the source section of the cell. The source was a 1/8-in.-diam tantalum U-tube mounted onto a copper block assembly. The flared fittings at each end of the U-tube provided a gas-tight connection for the source gas which flowed through the hollow electrodes. The electrodes were the electrical contacts for resistance heating of the tube. The copper block and flare fittings were cooled by water circulating in the 2-in.-diam stainless steel mounting tube shown in Fig. 2. The gas entered both ends of the source U-tube and expanded into the chamber from a 0.0135-in.-diam orifice drilled through the 0.006-in. tube wall. The

U-tube was surrounded by a copper cylinder, thermally connected to the water-cooled block. This acted as a radiation shroud to reduce the heat load on the cryosystem. The source temperature was determined by an optical pyrometer. This system had been calibrated in situ, and compared against gas temperatures as determined from velocity distribution measurements in previous experiments (Ref. 5).

As can be seen in Fig. 1, the gas addition system could be removed at any time by withdrawing it from the chamber and closing the 2-in. gate valve. The source orifice could be aligned from outside the cell by adjusting bolts on the steady rest. The pivot movement consisted of a stainless steel bellows enclosed in a gimbal assembly.

An operating pressure of $\approx 10^{-7}$ torr was maintained in the collimation section by a 10-in. oil diffusion pump and the GHe- and LN_2-cooled cryoliners. A small stream tube of the free-jet expansion in the source section was separated from the general flow field by a cryogenically cooled skimmer located at the entrance of the collimation section. The skimmer was a hollow cylinder with a 0.5-in.-diam hole which allowed passage of the gas into the collimation section. Gaseous helium at 20°K or liquid helium at 4.2°K was circulated within the cylinder which cryopumped the incident gas from the free-jet expansion. This type of skimmer eliminated the shock interactions reported by Brown and Heald for test runs with nitrogen (N_2) and argon (Ar)(Ref. 6). In runs with H_2, however, it was not successful. At the exit of the collimation section a second GHe-cooled cylinder with a 0.1875-in.-diam orifice collimated the gas stream so that a uniform monoenergetic molecular beam entered the test section.

In the test section vacuum conditions were maintained by a 10-in. diffusion pump and 20°K GHe-cooled cryopanels. An operating pressure of $\approx 10^{-8}$ torr was maintained in this section, which contained the beam detection system, the cryogenically cooled targets, and the associated mounting and drive mechanisms.

2.1.2 Detection Systems

The use of molecular beams for atomic and molecular interaction experiments has resulted in the development of several practical beam detection techniques (Ref. 7). One technique which aids in the discrimination between the beam signal and background noise is to modulate the molecular beam at a convenient frequency and then by ac amplification measure only that part of the signal which has the proper frequency and phase. This is generally referred to as modulated beam or lock-in detection. The technique is described in detail in Ref. 8. The system

used in these experiments combines the beam modulation technique with a quadrupole mass spectrometer as the detector. The use of the mass spectrometer further increases the signal-to-noise ratio by rejecting all gas species with mass numbers other than that to which it is specifically tuned.

The mass spectrometer was modified for use in two modes of operation. When the system was used for determining the spatial distribution of the molecular flux reflected from the test surfaces, a small box was attached to the head of the mass spectrometer. In this mode the gas molecules passed into the steady-state box through a small collimating hole before entering the ionization region of the mass spectrometer. Since the reflected molecules were brought to equilibrium with the walls of the box, the instrument responded only to changes in number density within the box which was in turn proportional to the molecular flow rate.

In the second mode of operation the system was used to determine the velocity distribution of the gas molecules. For these measurements the box was removed from the mass spectrometer and the standard ionization section was replaced with one which had an unobstructed opening. In this configuration the molecular pulses passed directly through the ionization region without striking any solid surface in the detection system, and the rate of ionization was proportional to the number density of the beam pulse in the ionization region at any instant in time.

The pulsed signal from the mass spectrometer was fed into a waveform eductor. This instrument and the data acquisition procedures have been described in Ref. 9.

An auxiliary detector in the form of a miniature ionization gage was used to monitor the total beam flux. This gage was enclosed in a glass envelope with a 0.25-in. orifice. A swing movement mechanism was used to lower the gage remotely into the incident beam for periodic checks on the beam intensity.

2.1.3 Target and Detector Movement Mechanisms

The target was mounted on the lower end of a cryogenic reservoir such that it could be rotated about an axis perpendicular to the incoming molecular beam. The target could be removed from the beam completely by raising the fill tube which penetrated the top of the chamber through an O-ring seal.

The mass spectrometer detector was mounted on a remotely operated turntable. All target and detector motions were provided by torque-motor and gear drive combinations. Precalibrated potentiometer and voltmeter systems coupled to these drive motors were used to indicate the detector location during experimental runs.

2.1.4 Target Substrate

The targets used in these experiments consisted of a section of aluminum cryopanel which had been cleaned by vapor blasting and a piece of an aluminum extruded cryopanel as received from the manufacturer. The latter target was also tested with a cryodeposit of CO_2 on its surface. The targets were welded at the outer edge to the target holder to ensure good thermal conductivity to the reservoir above it, and the temperature was maintained constant by either filling with water to hold the target at 300°K or with LN_2 to keep it at 77°K. Following these experiments a highly polished aluminum target was installed in the test cell. However, this target was not welded to the cryogenic reservoir and could not be cooled.

2.2 EXPERIMENTAL PROCEDURES

2.2.1 System Alignment and Calibration

The alignment of the skimmers, target, and detector system was performed with a laser beam and transit. The position indicators (potentiometer-voltmeter system) were calibrated against reference marks established in the test cell. The source orifice was aligned after the system was pumped down. This was accomplished by swinging the miniature ionization gage into the beam path. Then a small gas flow was started through the orifice and the clamping bolts on the steady rest adjusted to maximize the signal at the gage. It was found that this operation was necessary every time the source temperature was changed, since there was a slight warpage of the U-tube attributable to thermal expansion and contraction.

The total beam flux was obtained from

$$\dot{n} = \alpha (p_g - p_{bg})$$

where p_g is the measured pressure with the gage in the beam and p_{bg} is the background pressure with no beam. The calibration constant α(2.5 x 10^{20} molecules/sec-torr for argon (Ar), 3.1 x 10^{20} molecules/sec-torr for nitrogen (N_2), and 12 x 10^{20} molecules/sec-torr for

hydrogen (H_2)) was obtained by using an oven-type molecular beam to provide a known beam flux. This gage was not recalibrated before each day's experimental run. However, with source conditions repeated (i.e., source pressure, temperature, and orifice skimmer separation) the gage showed remarkable repeatability from day to day. This was accepted as sufficient indication that the gage sensitivity was not changing significantly.

2.2.2 Experimental Procedure for the Acquisition of the Spatial Reflected Flux Distribution Data

For these experiments the mass spectrometer was fitted with the closed box configuration. The desired target was mounted in the chamber and the system evacuated. The source was then slowly brought to operating temperature and a gas flow started. After alignment of the source by using the miniature ionization gage, the high-energy beam was allowed to impinge on the target. The mass spectrometer was then remotely manipulated to measure the reflected flux of molecules scattered from the target. The variables manipulated during this series of tests were as follows:

Gas specie	N_2, H_2
Gas temperature, T_o, °K	2900, 2000, 300
Angle of incidence, θ_i, deg	30, 45, 60
Target preparation	Vapor blasted, extruded, coated with cryodeposit, polished
Target temperature, T_t, °K	300, 77

2.2.3 Experimental Procedure for the Acquisition of the Reflected Velocity Distributions

For these experiments the mass spectrometer was modified by changing to the unobstructing ionization head. The flight distances from the chopper wheel to the target surface and from the target to the mass spectrometer were carefully measured before the chamber was closed and evacuated. After the molecular beam had been established and aligned the target was raised and the mass spectrometer was remotely adjusted so that the pulsed incident beam passed through its ionization section. The time-of-flight data were recorded in this position, and then the mass spectrometer was remotely moved through 180 deg until it was again on centerline with the incident beam but now located farther away from the source. A second set of time-of-flight data were recorded.

These two sets of data constituted a calibration run which provided information to calculate the rotating chopper shutter function and also the electronic delays in the various amplifiers and trigger circuits. The target was then lowered into the beam and set at the desired angle. As before the mass spectrometer was then remotely manipulated to record the time-of-flight signals at various angles of reflection. The variables in these experiments are shown below.

Incident gas (specie N_2, Ar; temperature 2200°K)

Target — Aluminum (vapor blasted)
(extruded)
(coated with CO_2 cryodeposit)
(coated with Ar cryodeposit)

Target temperature, T_t, °K: 300, 77, and 15

2.3 EXPERIMENTAL RESULTS

2.3.1 Reflected Spatial Distribution Data

The reflected spatial distributions of high-energy N_2 and H_2 are presented in this section. Since the in-plane data indicated very little departure from the cosine or random distribution patterns, no out-of-plane data were taken. (In-plane is defined by the vectors representing the molecular beam and the target surface normal.) Note that there is considerable scatter in the data presented for high temperature H_2. Therefore, the results obtained with this particular gas should be considered as preliminary and only indicative of its behavior. Further discussion of the problems encountered with H_2 and descriptions of specific experiments conducted to assist in assessing its behavior are included in Section III.

Aluminum Plate (Extruded)

This sample was cut from an extended fin on a section of an aluminum extrusion. This particular type of extrusion is used for fabricating cryoliners and radiation baffles. Since the extrusion process requires a fairly soft alloy, the 1100 series aluminum is used. No attempt was made to condition the surface of the sample. However, the section chosen was free of gross scratches and surface blemishes, and it was washed with acetone after it was installed in the system.

The reflected distributions from this sample are presented in Figs. 3 through 7. All the data, with the exception of those presented in Fig. 6, have been normalized so that reflected distributions could be more easily compared to a cosine distribution which is shown by the solid curve in each case.

Aluminum Plate (Vapor Blasted)

This target represents a typical aluminum cryopanel which has been cleaned by vapor blasting. This method of cleaning cryosystems has been used in the prototype rocket test cells. In addition to removing residues of fuel, oxidizers, and exhaust products, it leaves the soft aluminum cryopanels with a matte finish. The only additional treatment after mounting this sample was to wash it with acetone to remove any traces of grease or oil.

The reflected spatial distributions are presented in Figs. 8, 9, and 10. Closer examination of the data presented in Fig. 10 shows that the reflected molecular flux can be fitted to a cosine distribution if the actual surface normal is tilted backward slightly. Alignment of the beam and target assembly was rechecked, and it was determined that this was a real phenomenon and not an alignment problem. These tests were repeated for various angles of beam incidence and in each case the resulting reflected flux could be fitted with a cosine distribution by an appropriate choice of a "tilted surface normal." The angle at which the surface "normal" had to be tilted was defined as the roll-back angle, and a plot of this angle versus the angle of incidence is shown in Fig. 11. The evidence of backward scattering prompted additional tests with a highly polished aluminum target.

Aluminum Plate (Polished)

This target was made from a piece of 2024-T4 aluminum. The surface exposed to the molecular beam was hand polished to a mirror finish with jeweler's rouge and then washed with acetone. The data obtained from this surface are shown in Figs. 12 and 13. Data from previous work by Busby and Caldwell (unpublished) of an argon beam reflecting from a hand polished copper target cooled to 77°K are shown in Fig. 14. These data have been scaled so that they might be qualitatively compared to the trends observed with N_2 from aluminum.

2.3.2 Reflected Velocity Distribution Data

The reflected velocity distributions of high-energy N_2 from various surfaces are presented in this section. The beam intensities of the high-energy H_2 were too low to detect any reflected molecules from the

surfaces in this mode of operation. Figure 15 is representative of the time-of-flight pulse data which are taken to calculate the shutter function of the chopper wheel. A sample best fit curve as determined from the computer program along with the calculated shutter function at the target surface is shown in Fig. 16. Figure 17 is included to show representative data of the time-of-flight trace from a reflected pulse of molecules from a 300°K target. The summary of the velocity distribution data is presented in Fig. 18. The solid curves are the experimentally determined values of $\bar{v}$ and $\overline{v^2}$ plotted versus the angle of reflection. The dashed lines are the calculated values of $\bar{v}$ and $\overline{v^2}$ from classical kinetic theory assuming complete accommodation.

A series of experimental runs was made with Ar reflecting from an Ar cryolayer deposited on a 15°K surface. The results are presented in Fig. 19. These data were difficult to obtain because of the extremely low signal levels. Attempts to repeat the experiment using N_2 were not successful because the instrumentation was not sensitive enough to detect the reflected signal for this gas.

2.4 DISCUSSION

2.4.1 Spatial Distributions

The data obtained from the test runs with the extruded, vapor blasted, and CO_2 coated aluminum targets all exhibit a similar trend. Although the scatter in the data leaves the behavior of high-energy H_2 in some doubt, the 300°K H_2 as shown in Fig. 7 behaves very much like N_2. The basic scattering pattern is towards a cosine distribution. However, as can be seen in Figs. 8 and 9, there seems to be a suggestion of some backscattering. This seemed to be more pronounced for the large angle of incidence on the vapor blasted surface (Fig. 8). A comparison of reflected distributions for a fixed angle of incidence (60 deg) and for various gas temperatures indicates that the backscattering is more pronounced for the lower temperature gas (Fig. 9). A series of runs for 300°K N_2 impinging on the vapor blasted target at various angles was made. The plots for two of these angles are shown in detail in Fig. 10. As can be seen the reflected distribution can be fitted to an ideal cosine distribution if the axis is tilted slightly. Figure 11 presents a summary of this roll-back angle as a function of the angle of incidence of the molecular beam for six sets of data. Although it was felt that this was a true effect and not attributable to errors in alignment and calibration of incidence angles, an additional set of runs was made with a polished aluminum target. The data are presented in Fig. 12. The reflected distributions from this target show

no dependence on angle of incidence. However, it should be noted that when the source temperature was raised, the reflected distributions from this surface became lobular and were scattered in a forward direction (Fig. 13). Data from previous work involving scattering high temperature Ar from a polished copper surface show a similar forward lobular distribution (Fig. 14).

In retrospect it is suggested that the distributions shown in Figs. 3 through 9 are most likely a combination of a backward scattered component from surface roughness and a forward scattering tendency attributable to the high energy of the incident molecular beam, with the resulting near-cosine distribution being a fortuitous combination of the effects of surface roughness and beam energy.

2.4.2 Determination of Gross Energy Accommodation Coefficients

Overall energy accommodation coefficients were obtained by numerically integrating the reflected flux and velocity distribution data. It is recognized that the method used is a gross approximation, but the values provided are considered adequate for engineering calculations made to determine expected heat loads on cryoliners.

The velocity distribution data obtained for the incident high-energy gas beam show that the gas is nearly monoenergetic. Thus the total energy of a unit mass of gas incident on the surface is defined as

$$E_i = \frac{1}{2} M \overline{v_i^2}$$

where $\overline{v_i^2}$ is the mean square velocity of the incident beam.

Since the spatial distribution data indicated a near-cosine dispersion of the high-energy beam from engineering surfaces, the idealized case of a spherical distribution was used for the energy accommodation calculations. This distribution was then arbitrarily divided into six segments by radial planes. The fraction of the total mass (m_j) following through each segment was calculated from geometric consideration of the spatial distribution function and the two confining planes. Conservation of mass requires that $M = \sum_1^j m_j$. The total energy of the reflected molecules was calculated as

$$E_r = \sum_1^j \frac{1}{2} m_j \overline{v_j^2}$$

where $\overline{v_j^2}$ was determined from the data displayed in Fig. 18.

The energy accommodation coefficient is defined as

$$\epsilon = \frac{E_i - E_r}{E_i - E'_a}$$

where

$$E_a = \frac{1}{2} M \overline{v_a^2}$$

$$\overline{v_a^2} = \frac{4kT_s}{m}$$

T_s = surface temperature

m = mass of the gas atom

Thus, for the 2000°K N_2 reflecting from both the vapor blasted and extruded aluminum targets (300°K), the accommodation coefficient is calculated as 0.9. Similar calculations for the surfaces at 77°K yield values of ϵ essentially equal to unity. The trend shown in Fig. 18a indicates that for large angles of incidence (60 deg), those molecules leaving the surface at and above the specular angle are not so well accommodated. However, since these molecules represent only a small portion of the total reflected flux (determined from the spatial distribution plots) they do not significantly affect the gross accommodation coefficient.

When a beam of high-energy gas (N_2 or Ar) impinges on a cryopumping surface (15 to 20°K) the bulk of the gas sticks to the surface. However, it was previously noted by Caldwell and Busby that there are some molecules which are reflected from the target. The spatial distribution of these reflected molecules is discussed in Ref. 5. It can be seen in Fig. 19 that these molecules are leaving the surface with velocities that are much higher than expected for an evaporating flux, indicating that this phenomenon is not caused by a simple thermal overload of the cryosurface. It is interesting to note that, regardless of incident energy, the static temperature of the reflected beam determined from the half-width of the velocity distribution is about 36°K. This has previously been determined as the temperature at which condensation of Ar on a cooled substrate first begins. Since there are no data available for other gas species with significantly different vapor pressures this may be fortuitous.

More work is needed to better understand this phenomenon. The fraction of gas reflected is too small to be considered a problem in engineering applications, so these investigations were not pursued further.

SECTION III
OPERATION OF LHE CRYOPUMPS AT HIGH PRESSURES

3.1 APPARATUS

3.1.1 Vacuum Chamber

This work was performed in the AEDC-VKF 2- by 3-ft Research Vacuum Chamber described in detail in Ref. 10 and shown in Fig. 20. After deducting the space taken by the cylindrical cryopump and the liquid-nitrogen shrouds, the chamber has a free volume of 300 liters. The LN_2 shrouds are vented to allow free passage of gas molecules, yet they are optically tight between the outer chamber walls and cylindrical pump. The chamber is rough pumped by a 6-in. diffusion pump with an LN_2 cold trap. This system can be valved off with a 6-in. gate valve. A 2-in.-diam thin-walled orifice installed between the chamber and the diffusion pump is used as a secondary calibration standard for checking gage sensitivities during test sequence.

3.1.2 Cylindrical Cryopump

The cylindrical cryopump (Fig. 21) is a 5-in.-diam by 10-in.-high stainless steel cylinder. The pump is mounted to a low-heat-leak fill tube, and the upper half is surrounded by a radiation shield. This shield also serves to limit the pumping to the lower half of the cylinder. The pump will hold a total of 3.5 liters of cryogenic fluid.

The transfer line is a quad-concentric line which serves as a supply for the LHe and also as the vent line for the boil-off gas. This type of transfer line has been used in previous applications in this laboratory and has proven to be extremely efficient when used for LHe transfer. The details of construction can be found in Ref. 4.

3.1.3 Gas Addition Systems

Associated with the chamber are two gas addition systems. The first is used as a calibration system to determine the ion gage sensitivity factor over the pressure ranges that will be used in subsequent

tests. This system uses a set of sintered steel leaks which may be calibrated in situ. Details of this system may be found in Ref. 11. The gas addition tube enters the chamber and ends outside the LN_2-cooled shroud. Gas added has to diffuse through the optically tight but open shroud before reaching the gage. The second system consists of a reservoir, flowmeter (rotometer), and needle valve. This system supplies gas to a gas addition tube which penetrates the shroud and ends with a well-defined 0.017-in.-diam thin wall orifice which faces the bottom of the cylindrical cryopump. This tube is movable, so that the distance between the orifice and the bottom of the pump can be varied. The tube also can be rotated so that the orifice can be positioned behind a baffle attached to the shroud (Fig. 20). When the orifice is located behind the baffle all the gas added to the chamber is completely randomized before being pumped.

3.1.4 Instrumentation

Pressures in the chamber were monitored by an ionization gage connected to a short tube which penetrated the radiation shroud. A small baffle located at the entrance to the tube prevented any gas molecules from the gas addition orifice directly entering the gage regardless of the orifice location. The ion gage thus sampled the same random gas flux pumped by the LHe pump.

Flow rates of the test gas into the chamber during pumping runs were measured with a rotometer, and gas pressures in the supply reservoirs were monitored with aneroid-type pressure gages.

The boil-off rate of the LHe from the pumping system was measured by routing the venting gaseous helium through a warmup coil and then through a wet test meter. Time intervals were taken with a stop watch.

3.2 CALIBRATION

3.2.1 Leak System

Each leak in the gas addition systems was calibrated for the gases used. The method consisted of monitoring the rate of pressure drop in the known volume reservoir as the gas flowed from this volume through the leak and into the vacuum chamber. Pressures in the reservoir were in the millimeter range and were recorded by instruments calibrated against mercury standards. Full details of this procedure and analysis of the method are included in Ref. 11.

3.2.2 Gage Calibration

The ion gage was calibrated by comparing the recorded rate of rise of pressure in the vacuum chamber with a known rate of gas being admitted via the calibrated leak system. During these runs, all pumping systems were valved off and the radiation shrouds were at room temperature. Calibration factors for H_2 were determined for all scale ranges from 10^{-6} to 10^{-3} torr. This method of calibration is outlined in detail in Ref. 11.

3.3 EXPERIMENTAL PROCEDURES

3.3.1 Preparation for Test Run

The chamber was pumped down to its base pressure using the diffusion pumping system. Then LN_2 was transferred to the cryopump until it was filled. The chamber was then allowed to stand for 24 hr. During this period the boil-off gaseous nitrogen from the pump was routed through the wet test meter, and the cumulative total of gas evolved was recorded. When this record indicated that approximately 250 cc of LN_2 remained in the pump, the wet test meter was disconnected and a mechanical forepump was attached to the boil-off vent. As the pressure was reduced over the LN_2 it slowly subcooled the pump assembly. During this subcooling process liquid-nitrogen flow was started through all the radiation shrouds. The pressure over the LN_2 in the pump assembly was monitored with a thermocouple-type pressure gage. A rapid pressure drop to the base pressure of the mechanical forepump (30 microns) indicated that all the LN_2 had evaporated in the pump assembly. At this point the forepump was disconnected and the cryopump was pressurized to 15 psia with helium gas. The liquid-helium dewar was then connected to the transfer line and LHe was transferred to the cryopump. After the cryopump was filled, the LHe valve was closed and the tare heat load attributable to radiation and thermal conduction was determined by measuring the gaseous-helium boil-off rate with the wet test meter. The gate valve to the diffusion pump system was then closed.

3.3.2 Determination of Capture Coefficient for Random Incidence

The movable gas addition orifice was located behind the baffle assembly. Hydrogen was then admitted to the chamber through the rotometer gas addition system. The resulting steady-state chamber pressures for various gas addition rates were recorded. Since in this mode of operation all the gas molecules incident on the pumping surface must have had at least two collisions with LN_2-cooled surfaces it is assumed that the H_2 can be considered random and precooled to 77°K. If one considers the

gas flow in units of torr-liters/sec, then gas flowing into the system and that being pumped can be equated when a constant chamber pressure is indicated by the ion gage. Since these units implicitly include a temperature term then this equality may be written

$$\frac{Q_{300\ (in)}}{300} = \frac{Q_{77\ (out)}}{77} \tag{1}$$

where Q is the flow rate in torr-liters/sec and the subscripts 300 and 77 are used to designate the temperature (Ref. 12).

The term $Q_{77(out)}$ may be represented by a rate of strike at the pumping surface (S_{77}) multiplied by a sticking probability (c) and the chamber steady-state pressure (p_{77}). Thus

$$Q_{77(out)} = c\ p_{77}\ S_{77} \tag{2}$$

Combining Eqs. (1) and (2)

$$Q_{300(in)} = \frac{300}{77}\ (c\ p_{77}\ S_{77})$$

However, the pressure in the chamber is measured with a gage which has been calibrated at 300°K. Therefore, since

$$p_{77} = \beta_{300}\sqrt{\frac{77}{300}}\ p_g$$

where β_{300} is the gage calibration factor for H_2 determined at 300°K and p_g is the gage reading, and

$$S_{77} = \sqrt{\frac{77}{300}}\ S_{300}$$

then

$$Q_{300(in)} = c\ \beta_{300}\ p_g\ S_{300}$$

and

$$c = \frac{Q_{300(in)}}{\beta_{300}\ p_g\ S_{300}}$$

By calibrating the gage at room temperature, all calculations of flow rates may be made for room temperature conditions and no thermal transpiration correction terms are required, even though the experiments were conducted within a 77°K radiation shroud.

3.3.3 Determination of Capture Coefficient for Directed Incidence

This series of tests was conducted with the orifice located directly below the cryopump cylinder. Thus a portion of the expanding gas flow impinged directly on the LHe-cooled surface. The remainder of the flow had at least one collision with the LN_2-cooled shroud before returning and cryopumping with random incidence. The tests were conducted with the orifice first located 5 in. from the surface and then 2.75 in. At each position several gas flow rates were initiated and maintained until a steady-state pressure reading was recorded by the ion gage.

The following analysis was used to determine the capture coefficient of the incident gas flow. Let Q^* be the flow rate through the orifice and ξ be the fraction of the directed flow incident on the pump surface. If c^* is the capture coefficient for the directed flow then the quantity of gas which maintains the chamber pressure is a summation of $Q^*\xi(1-c^*)$, which is the reflected fraction from the pumping surface, and $Q^*(1-\xi)$, which is the fraction which does not encounter the front surface of the pump. Therefore, the gas load which randomly cryopumps on the LHe surfaces and maintains the steady-state chamber pressure is

$$Q^*(1-c^*\xi)$$

This random gas load can be compared to gas loads from the previous experiments where the orifice was located behind the baffle. Therefore, for directed flow

$$Q^*(1-c^*\xi) = c\,\beta_{300}\,p_g^*\,S_{300} \tag{3}$$

and for random flow

$$Q = c\,\beta_{300}\,p_g\,S_{300} \tag{4}$$

where terms with asterisks represent data for the directed flow experiment. Dividing Eq. (3) by Eq. (4) yields

$$\frac{Q^*}{Q}(1-c^*\xi) = \frac{p_g^*}{p_g}$$

and solving for c*

$$c^* = \left(1 - \frac{p_g^*}{p_g}\frac{Q}{Q^*}\right)\frac{1}{\xi}$$

3.3.4 Measurement of Heat Loads

During the tests which were conducted to determine the pumping characteristics of the H_2 on the LHe-cooled cryopump, the boil-off rates of the gaseous helium were measured. Since the gaseous helium immediately entered the vent section of the transfer line it was assumed that only the latent heat of vaporization of the LHe was absorbed from the heat load impinging on the pump. Thus, conversion of the gaseous-helium evolution rate to a liquid-helium boil-off rate led to a direct measurement of the total heat load on the pump.

SECTION IV
RESULTS AND DISCUSSION

In order to determine the capture coefficient of gas randomly incident on the cryosurface it was necessary to calibrate the ion gage over the pressure ranges which would be experienced in the pumping tests. Figure 22 shows the importance of calibrating the gage rather than accepting the manufacturer's recommended gage sensitivity factor. There was a considerable offset between the 10^{-5} and 10^{-4} torr scales and a step shift in sensitivity at the upper end of the 10^{-4} scale. This sensitivity shift is characteristic of this type of gage and can be attributed to a change in the mode of ionization at this pressure level. Analysis of the data obtained in the 10^{-5} torr range shows a capture coefficient of 0.94. In the range from 10^{-4} to 2×10^{-3} torr the capture coefficient is calculated as 0.96. Thus, for practical purposes, the capture coefficient appears to remain close to 1.0 for randomly incident 77°K H_2 impinging on LHe-cooled surfaces at pressure levels up to 2.0×10^{-3} torr.

The mass fraction of the H_2 gas incident on the pump face in the directed flow tests was determined from a method of characteristics flow-field analysis. Results from these computer-determined flow fields for a sonic orifice are shown in Fig. 23. Using the appropriate mass fractions for orifice pump separation distances of 2.75 and 5.0 in., the primary capture coefficients were calculated for various flow rates.

Figure 24 summarizes these results. At low incidence rates it can be seen that the capture coefficient is not greatly different from that measured for random incidence pumping. However, as the mass flow is increased the capture coefficient rapidly drops to zero. At flow rates higher than those recorded in Fig. 24 the capture coefficient becomes negative, which indicates that gas which had already been cryopumped is being eroded and adding to the background gas load.

Although the gas incidence rate is not exactly uniform over the pump surface, it is interesting to note that the incidence rate at which the capture coefficient goes to zero is approximately the same for both orifice to pump separation distances. This incidence rate is on the average 2.8×10^{-6} gm/sec-cm^2. The expected heat of condensation from 300°K H_2, cryopumping at this rate is calculated at 1.1×10^{-2} w/cm^2, giving a total heat load on the pump of approximately 1.5 w. This value is close to the experimentally determined heat load of 1.2 w obtained from gaseous-helium boil-off rates.

Using a value of 0.0025 w/cm-sec for the thermal conductivity of stainless steel one can estimate that temperature gradients as high as 1.4°K can exist between the LHe and the cryodeposit on the face of the pump at these heat loads. It is therefore suggested that the pumping limitations in these tests may be strongly influenced by the thermal properties of the stainless steel.

It was noted that the heat load, as measured by the liquid-helium boil-off rate, did not return to the quiescent value as rapidly as expected after high gas flow rates (>5×10^{-4} gm/sec) were terminated. When the H_2 flow was stopped the pressure in the cell dropped rapidly, indicating that the condensation heat load had dropped to near zero. However, as is shown in two examples plotted in Fig. 25, it took several minutes for the heat load to decay to the tare value. This presents additional evidence that the base plate of the pump acted as a heat sink and slowly warmed up during the pumping process.

A second set of direct incidence pumping data was obtained at the end of a test run where 4.5 gm of H_2 was already cryopumped on the LHe surface. These data have been reduced to determine capture coefficients and are included in Fig. 24. As can be seen, there is no significant difference in the values recorded. Since the density of the H_2 cryofrost is not known, no estimate of the cryofrost thickness can be made. However, the results indicate that the thermal gradients across this cryodeposit are not significant. This is in contrast to previous H_2 cryopumping work where an aluminum cryosurface was used. In those

studies the poor pumping characteristics were ascribed to an exceptionally low thermal conductivity of the H_2 frost. It is possible that the problem with the aluminum substrate may have been caused by poor adhesion of the cryofrost to the cryosurface. This would have resulted in an apparently lower value of the thermal conductivity of the frost. During the studies with H_2 on a stainless steel cryosurface there was no sign of poor adhesion or flaking of the frost layer. It is not fully understood what factors determine the cryodeposit structure. It has been noted during these tests that high incidence rates tend to produce a porous snowlike deposit. However, on occasion, glassy icelike cryodeposits were formed with no apparent change in any of the chamber conditions. Several general observations can be made after testing N_2, Ar, H_2, CO_2, H_2O, and NH_3 condensing on copper, stainless steel, and aluminum cryopanels cooled to the appropriate temperatures. First, Ar seems to be the best behaved gas, condensing equally well on all cryopanels and producing a glassy cryodeposit that adheres well to the substrate. H_2 and CO_2 are the worst behaved gases of those tested, especially when condensed on aluminum and copper cryosurfaces. It is suggested that problems of peeling and separation may be a result of differences in the thermal expansion of the cryodeposit and the cryosurface. Thermal loads attributable to either the heat of condensation of additional gas or radiation from a heat source tube cause the cryodeposit to warm up slightly and expand. However, the thermal conductivity of the copper and aluminum cryopanels is high enough that their temperature remains constant and thus they stay dimensionally stable. The reason that frosts seem to adhere better to stainless steel may be because its thermal conductivity is quite poor at these low temperatures and therefore it also warms and expands along with the cryodeposit.

SECTION V
SUMMARY

The results of the tests indicate that for surfaces such as those used in the construction of cryopanels and baffles, the high energy gases are reflected with a near-cosine distribution. In addition it was found that high-energy N_2 and H_2 were also reflected with a near-cosine distribution from cryosurfaces previously coated with a cryodeposit. Lobular distributions were obtained with high-energy incident gas beams reflecting from highly polished surfaces. However, it is impractical to consider a large test facility with cryopanels finished to such mirror surfaces in order to take advantage of any possible molecular focusing effects.

The data taken to determine the energy accommodation of high-energy plume gases on cooled surfaces show that for engineering purposes the plume gases can be taken to be fully accommodated if they suffer at least one collision with the surface.

The work conducted with H_2 has helped to define the problem areas and has provided some guidelines for using available pumping techniques. However, there are still major problems in pumping this gas. These studies have shown that, for precooled and thus randomly incident H_2, capture coefficients close to unity can be realized for chamber pressures up to 10^{-3} torr on LHe-cooled surfaces (4.2°K). Under these conditions the pumping does not seem to be influenced by the cryopanel material (i.e., copper, aluminum, or stainless steel). For directed flows of H_2 on liquid-helium-cooled surfaces the limitations are apparently caused by heat loads from the heat of condensation of the H_2 itself and by radiation heat load from the 2000°K supply tube in the high-energy studies. In the case of stainless steel the upper limit of operation is primarily determined by its poor thermal conductivity, whereas for copper and aluminum the upper limit is apparently determined by differences in the thermal expansion of the cryofrost and the cryosurface.

It is suggested that future work should include a closer study of the factors influencing the cryofrost structure, with emphasis on the cryofrost and cryopanel interface.

REFERENCES

1. Ruby, E. C., Brown, R. F., Busby, M. R. "The Effects of Condensation on the Flow Field Properties in Free-Jet Expansions of Argon." AEDC-TR-70-142 (AD710616), August 1970.

2. Benek, J. A. "Prediction of Molecular Scattering Effects in Free-Jet Expansions." AEDC-TR-70-273 (AD717158), January 1971.

3. Chubb, J. N. and Pollard, I. E. "Experimental Studies of H_2 Condensing on LHe Cooled Surfaces." Vacuum, Vol. 15, No. 10, October 1965.

4. Dawbarn, R. and Haygood, J. D. "Development and Evaluation of a Cryodeposit Sorption Pump Capable of Pumping Helium." AEDC-TR-68-90, September 1968.

5. Arnold, F., Busby, M. R. and Dawbarn, R. "Experimental Investigation of the Scattering of a Nitrogen Aerodynamic Molecular Beam from a Solid Nitrogen Surface." AEDC-TR-70-172 (AD712374), October 1970.

6. Brown, R. F. and Heald, J. H., Jr. "Description and Performance of a Molecular Beam Chamber Used for Cryopumping and Adsorption Pumping Studies." AEDC-TR-66-135 (AD641388), October 1968.

7. Trischka, J. W. Methods of Experimental Physics 3: Molecular Physics. Ed. by D. Williams, Academic Press, New York, New York, 1962.

8. Fite, W. L. and Datz, S. "Chemical Research with Molecular Beams." Annual Review of Physical Chemistry, Annual Reviews, Inc., Stanford, California, Vol. 14, 1963, pp. 61-68.

9. Powell, H. M. and Heald, J. H., Jr. "A System for the Measurement of Velocity Distributions of Molecular Beams." AEDC-TR-68-151 (AD675306), September 1968.

10. Haygood, J. D. and Dawbarn, R. "Helium Pumping by 4.2°K Cryodeposits." AEDC-TR-66-204 (AD645511), January 1967.

11. Dawbarn, R. "Cryosorption of H_2 by 12 - 20°K Carbon Dioxide Cryodeposits." AEDC-TR-67-125 (AD655067), July 1967.

12. Dushman, S. Scientific Foundations of Vacuum Technique. John Wiley and Sons, Inc., New York, May 1955.

APPENDIX
ILLUSTRATIONS

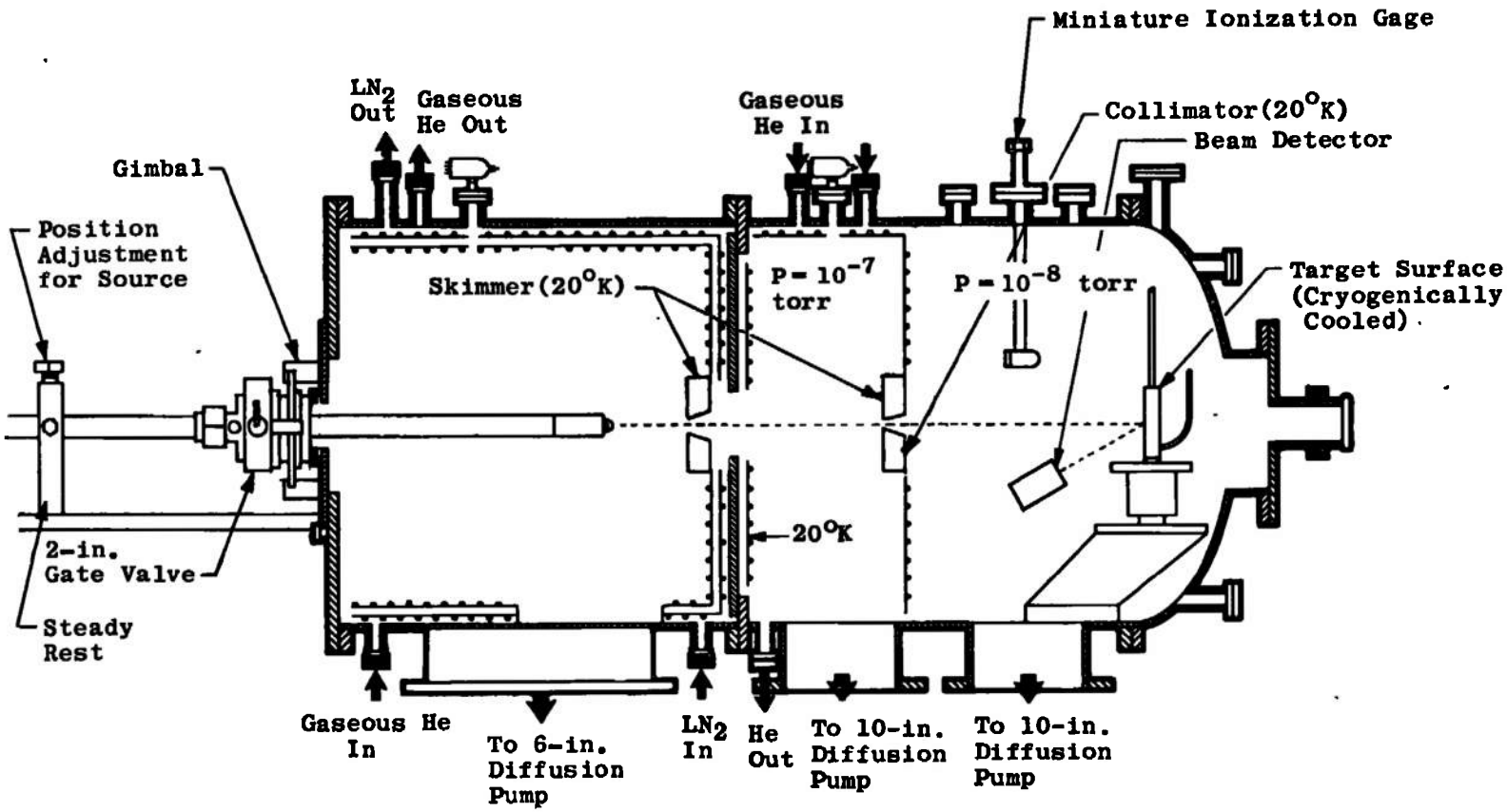

Fig. 2 Aerodynamic Molecular Beam Chamber

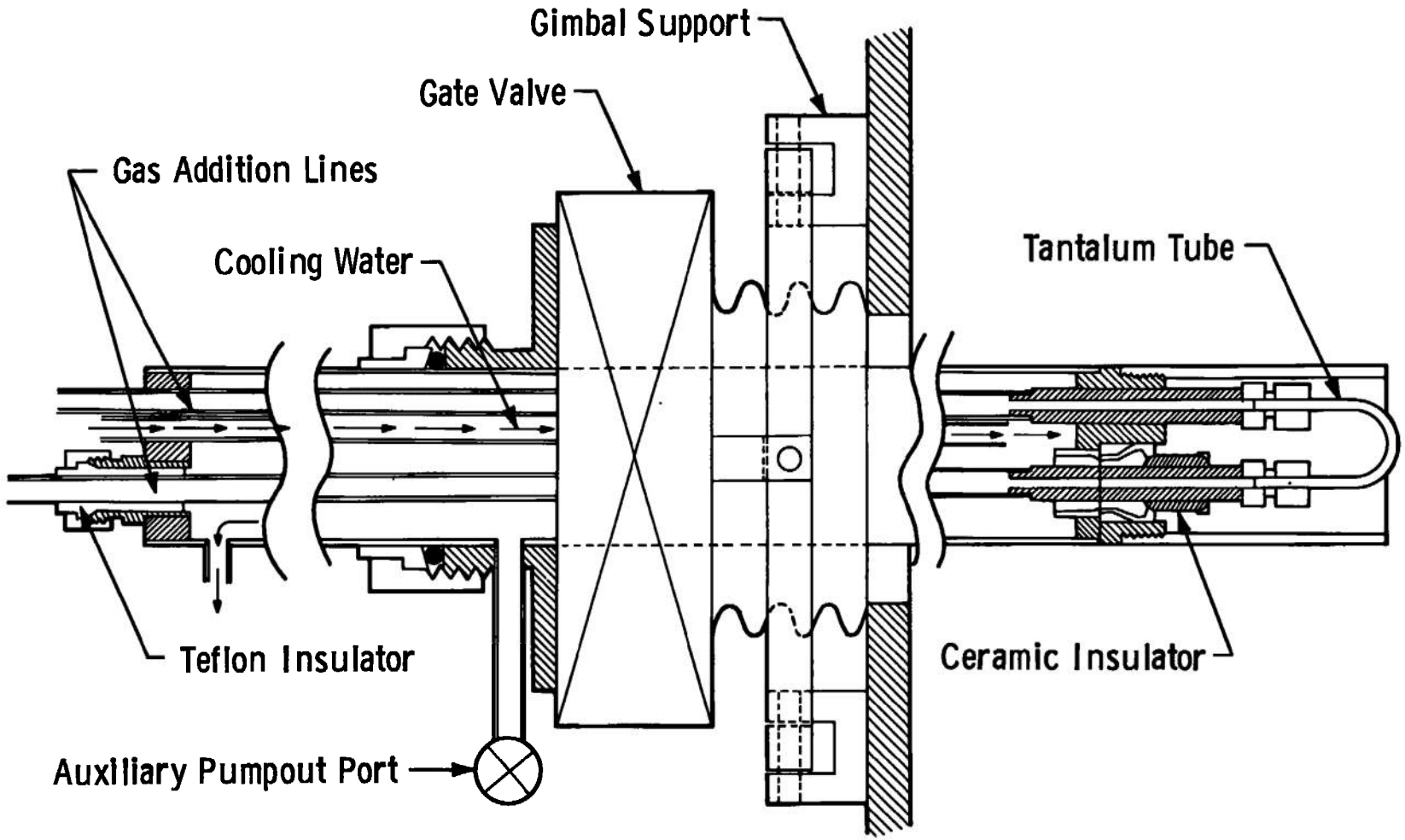

Fig. 2 Schematic of High Temperature Gas Addition System

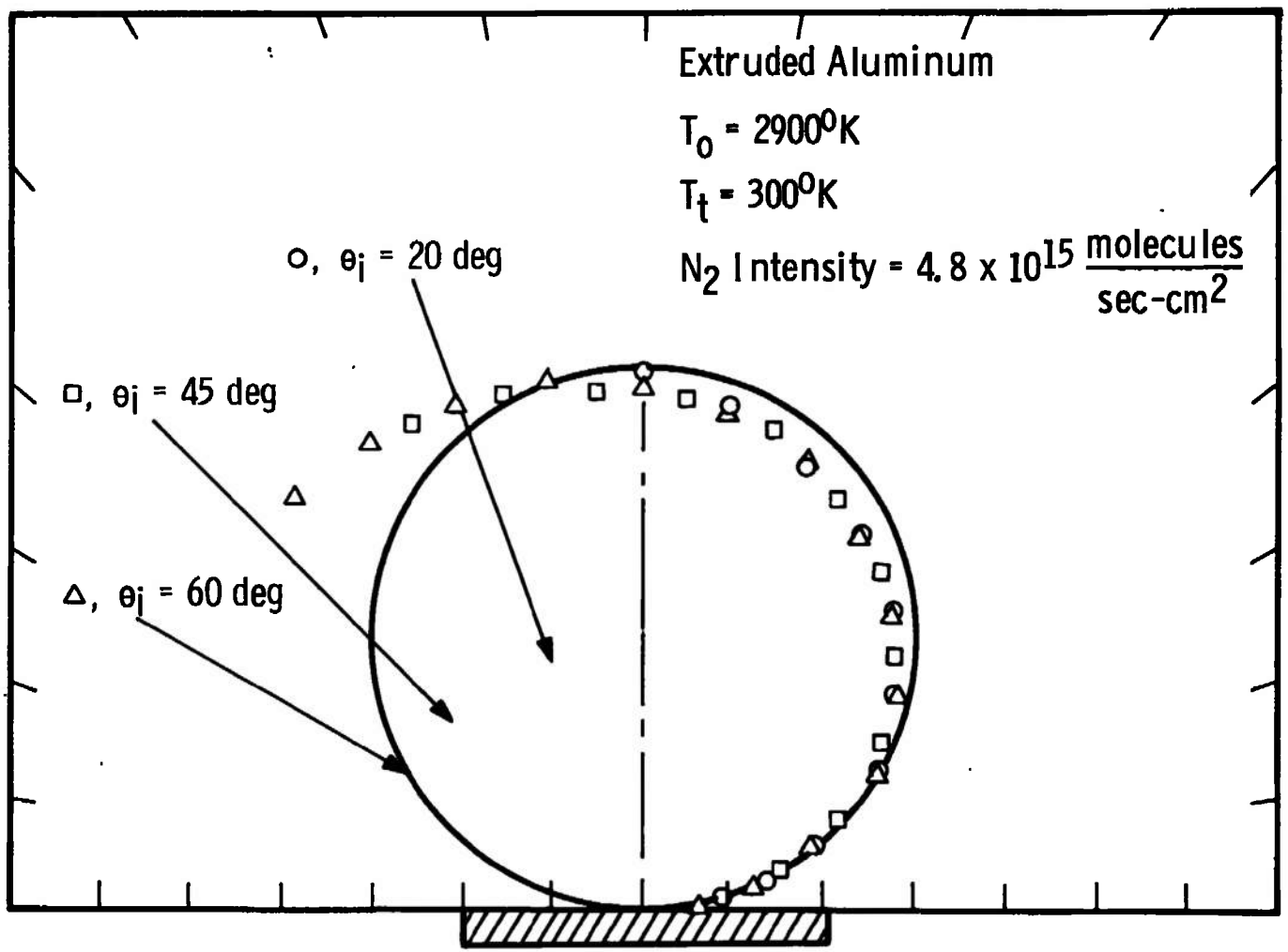

Fig. 3 Reflected Spatial Distribution of N_2 from a 300°K Extruded Aluminum Surface

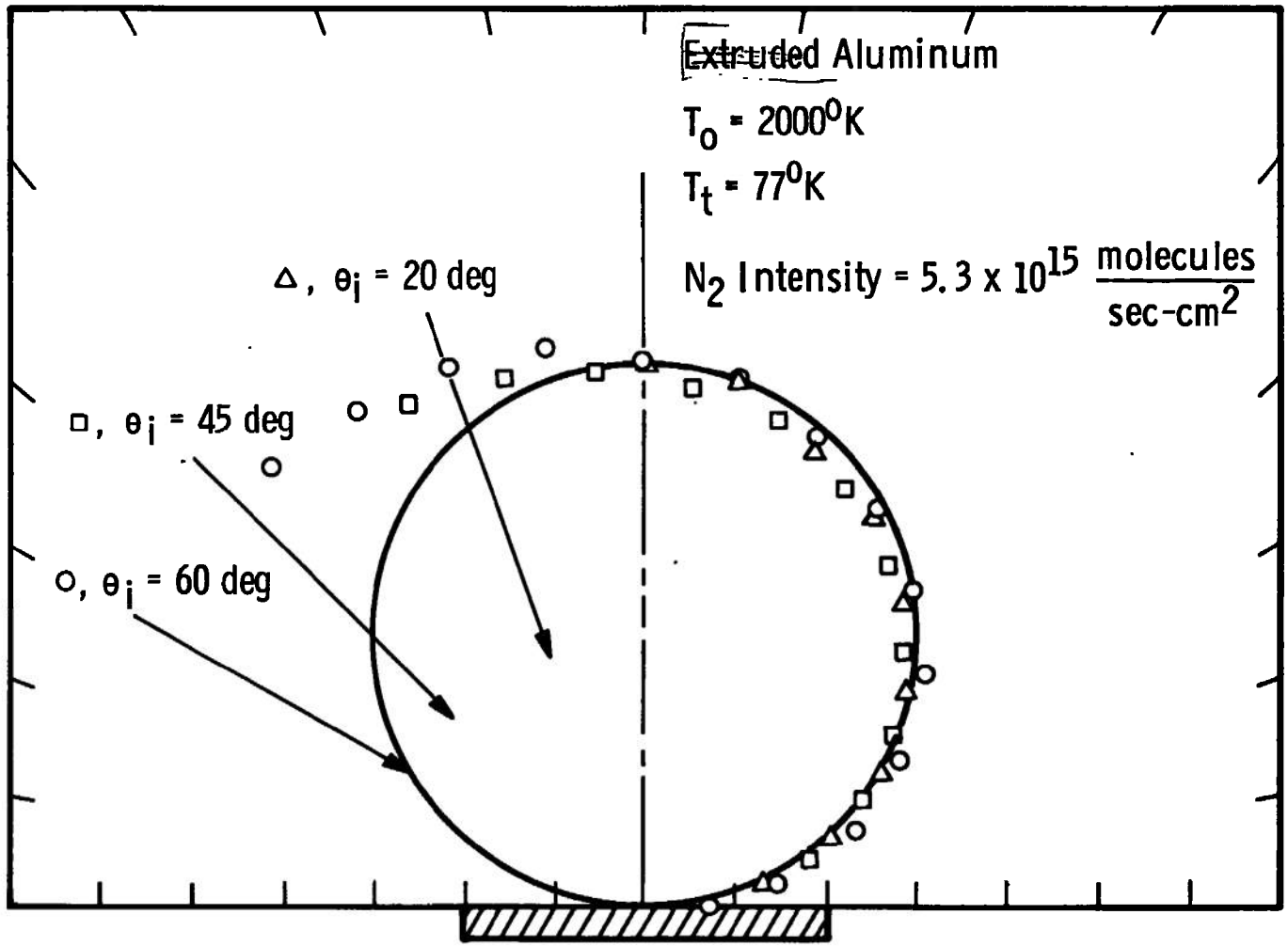

Figure 89 Spatial Distribution of Nitrogen Reflected from a 77°K Surface.

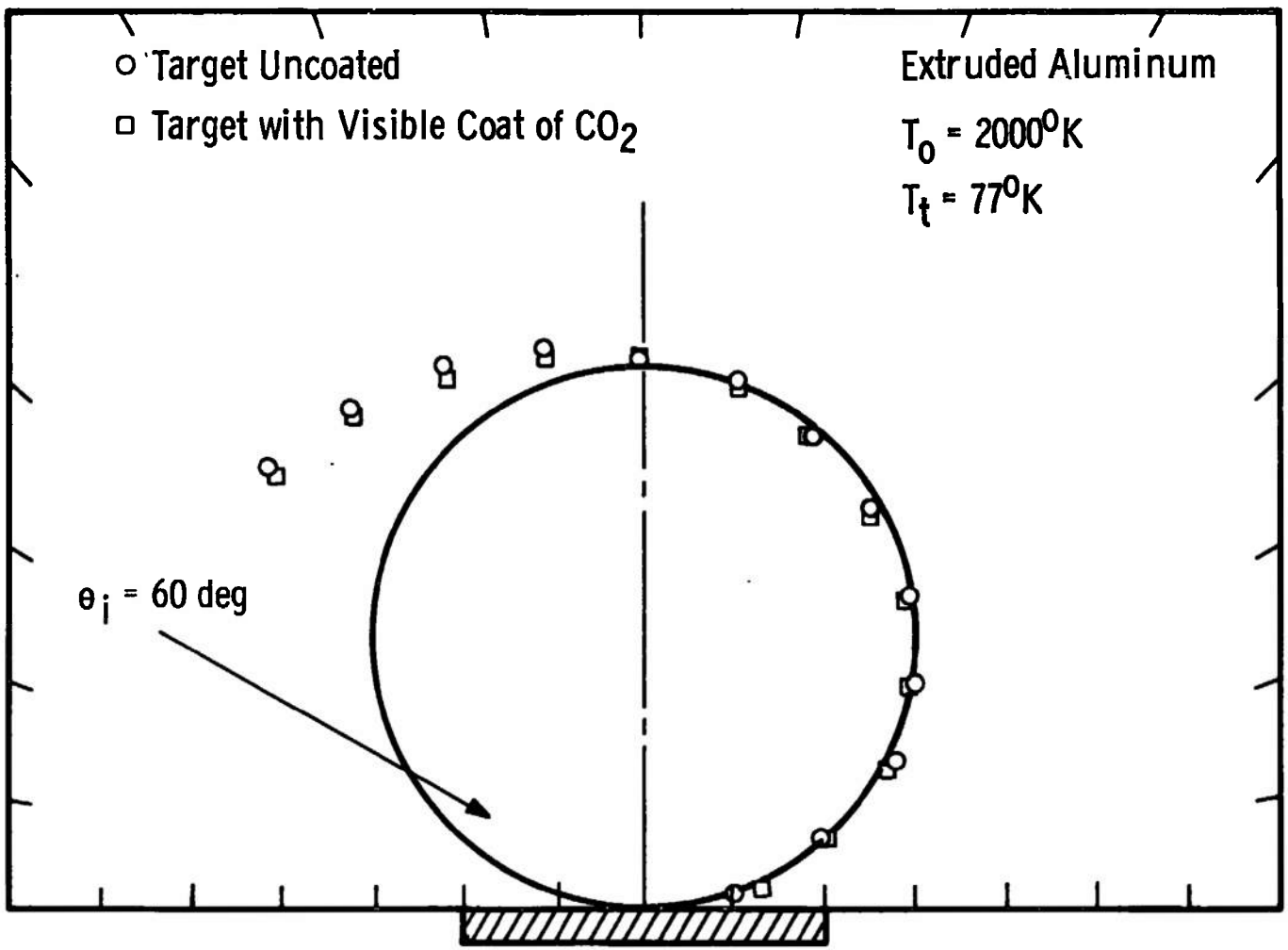

Fig. 5 Reflected Spatial Distribution of N_2 from a 77°K Extruded Aluminum Surface Coated with CO_2

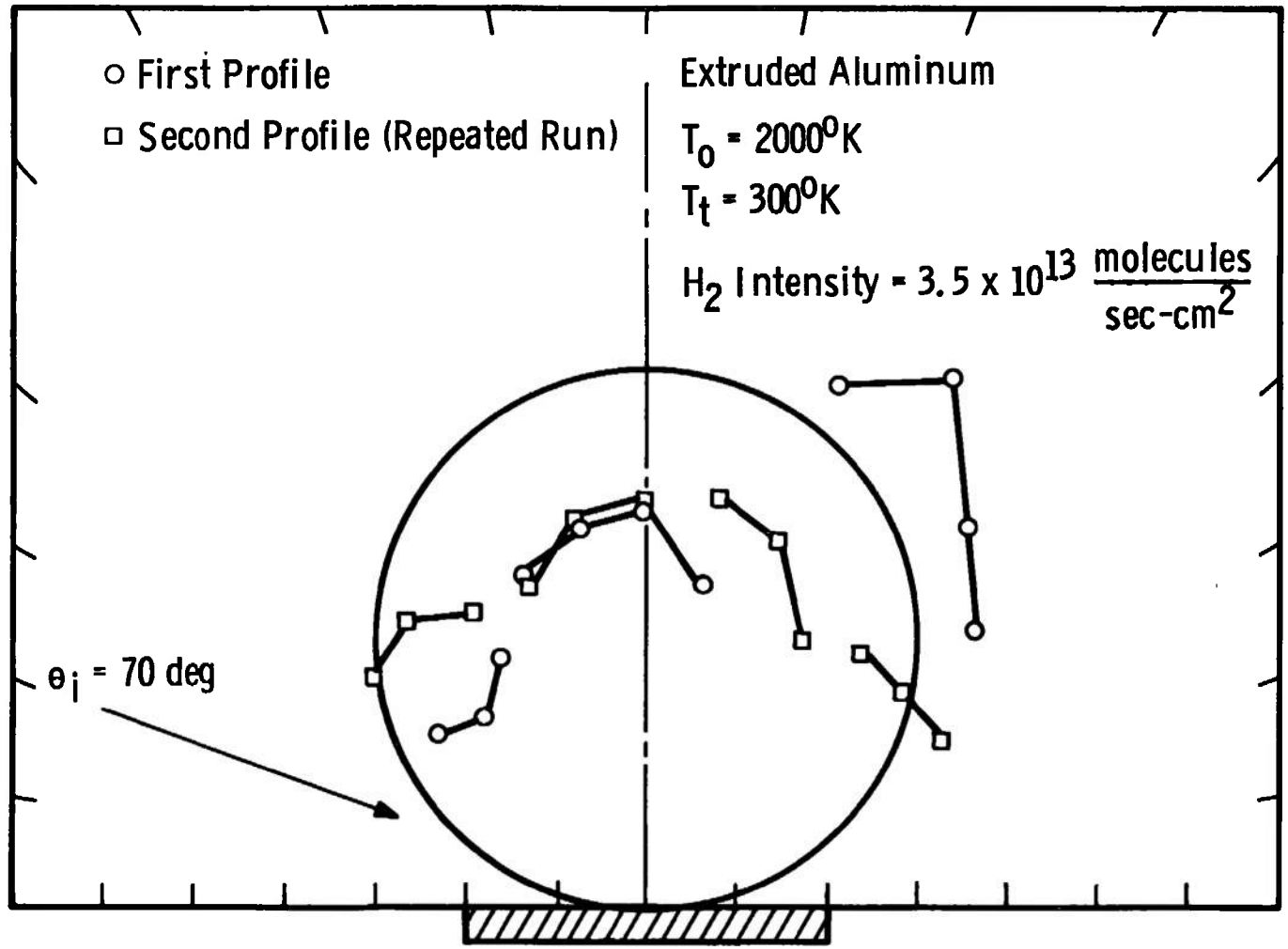

Fig. 6 Reflected Spatial Distribution of H_2 from a 300°K Extruded Aluminum Surface

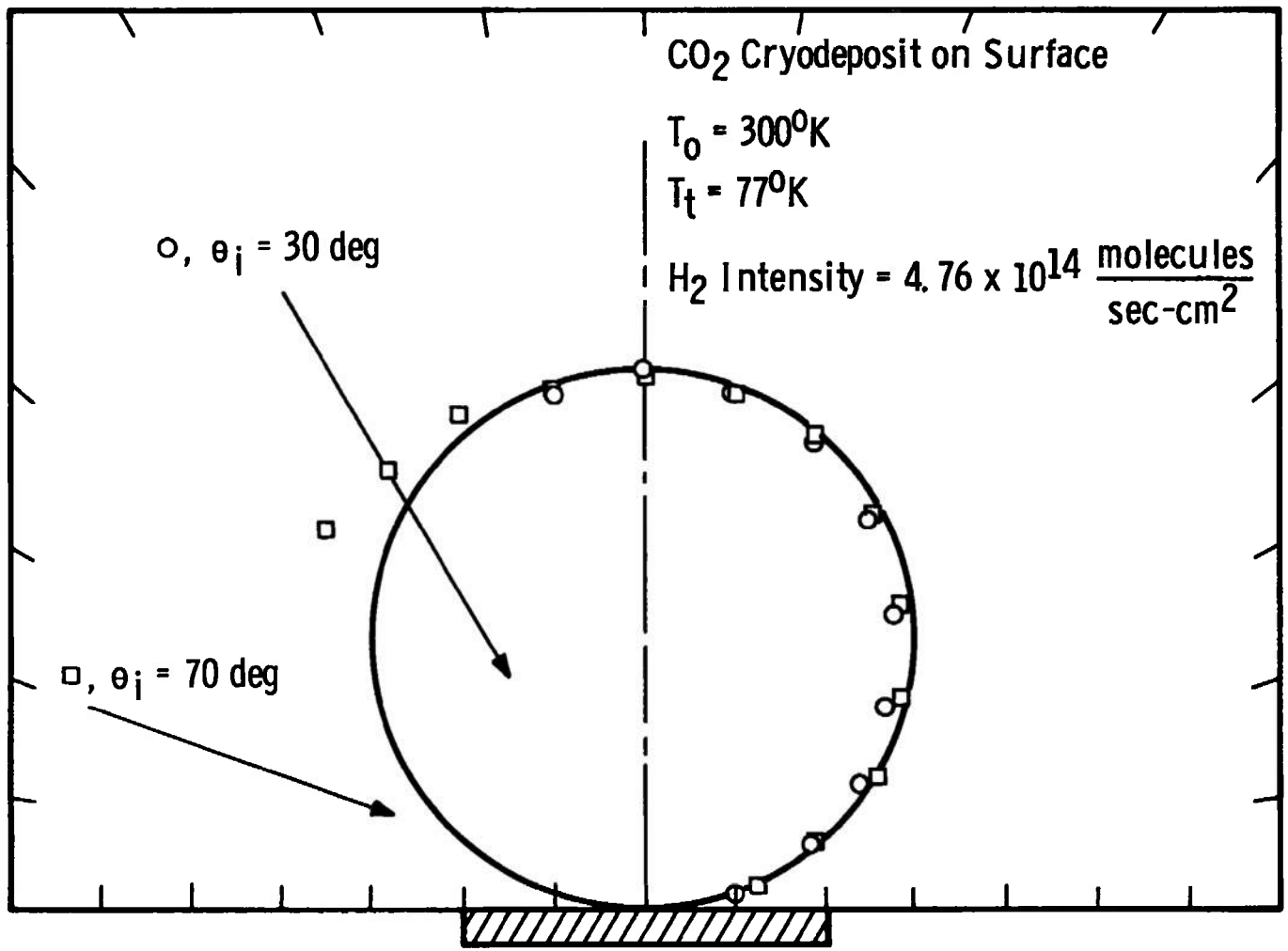

Fig. 7 Reflected Spatial Distribution of H_2 from a CO_2 Cryodeposit on an Extruded Aluminum Surface

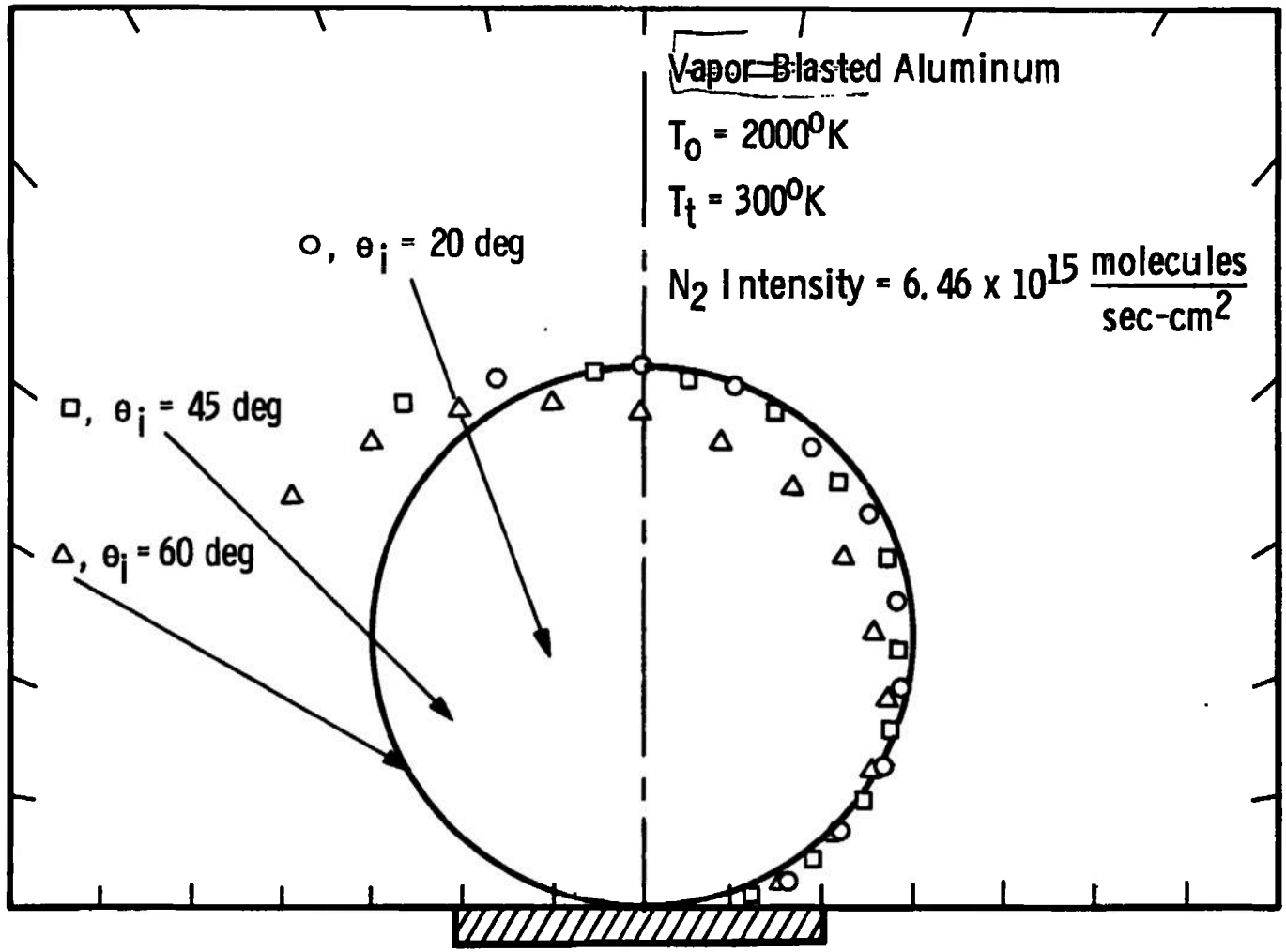

Figure 18. Spatial Distribution of Nitrogen Reflected from a 300°K Surface.

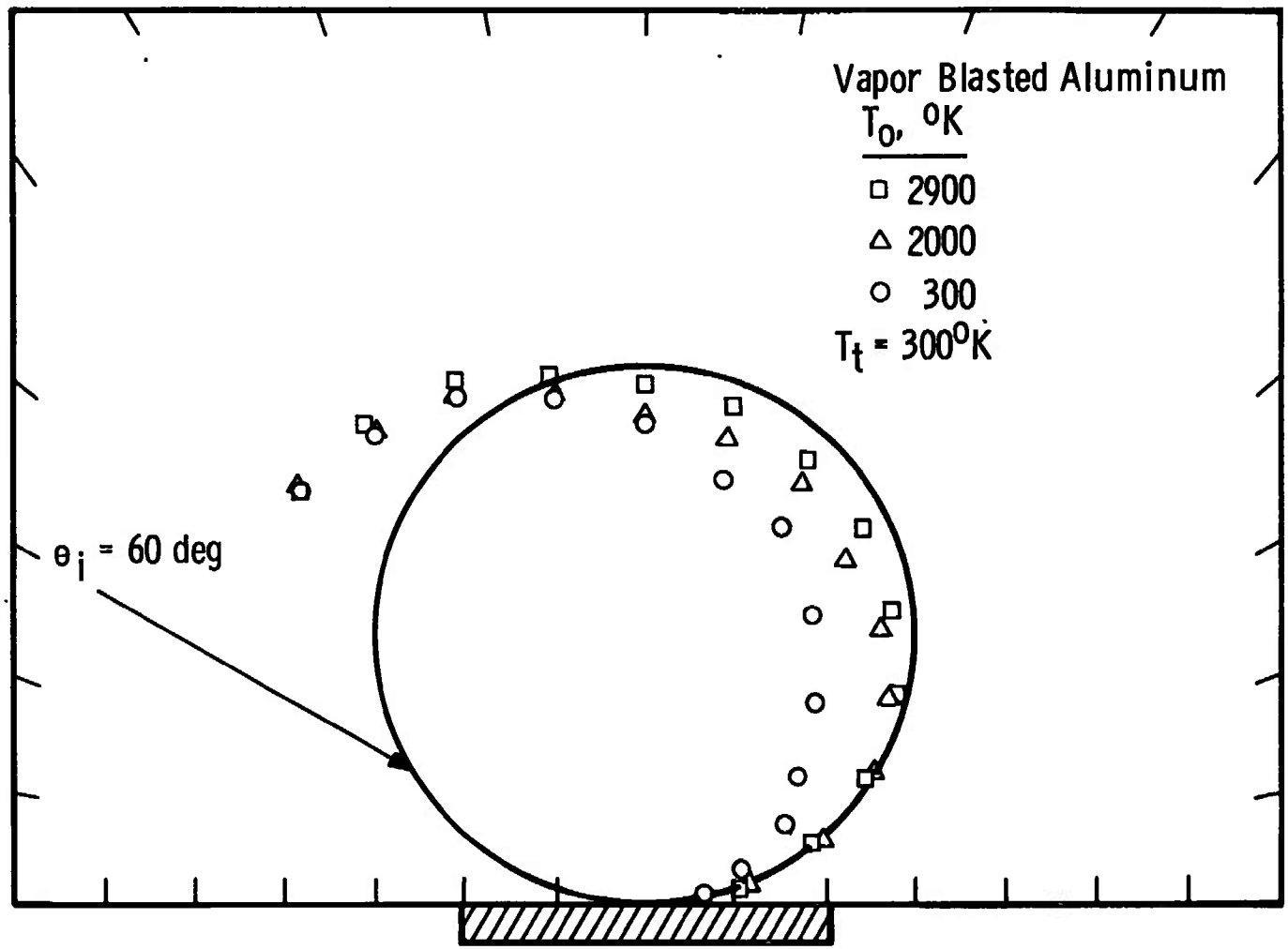

Fig. 9 Reflected Spatial Distribution of N_2 from a 300°K Vapor Blasted Aluminum Surface for Various Incident Energies

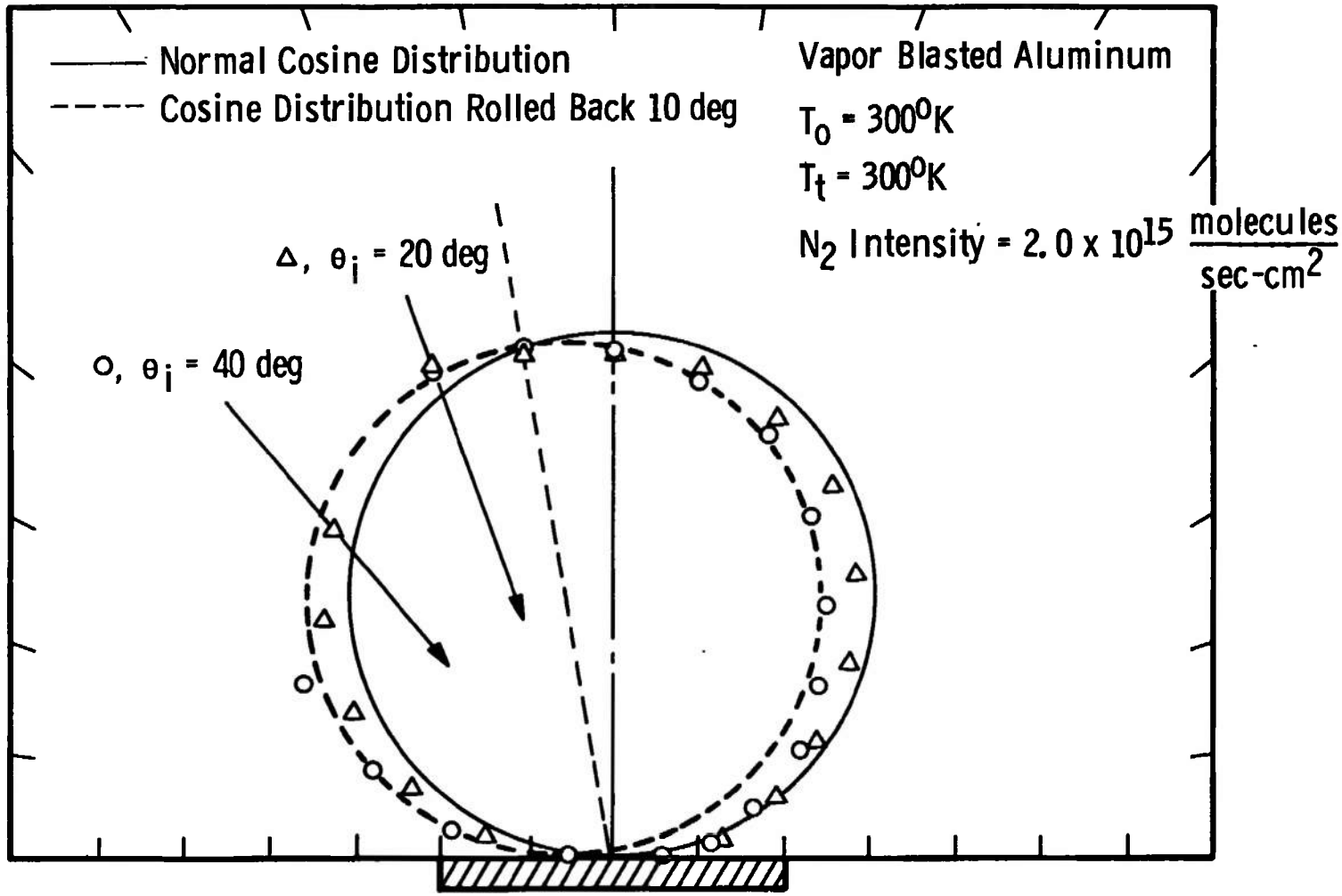

Fig. 10 Reflected Spatial Distribution of 300°K N_2 from a 300°K Vapor Blasted Aluminum Surface

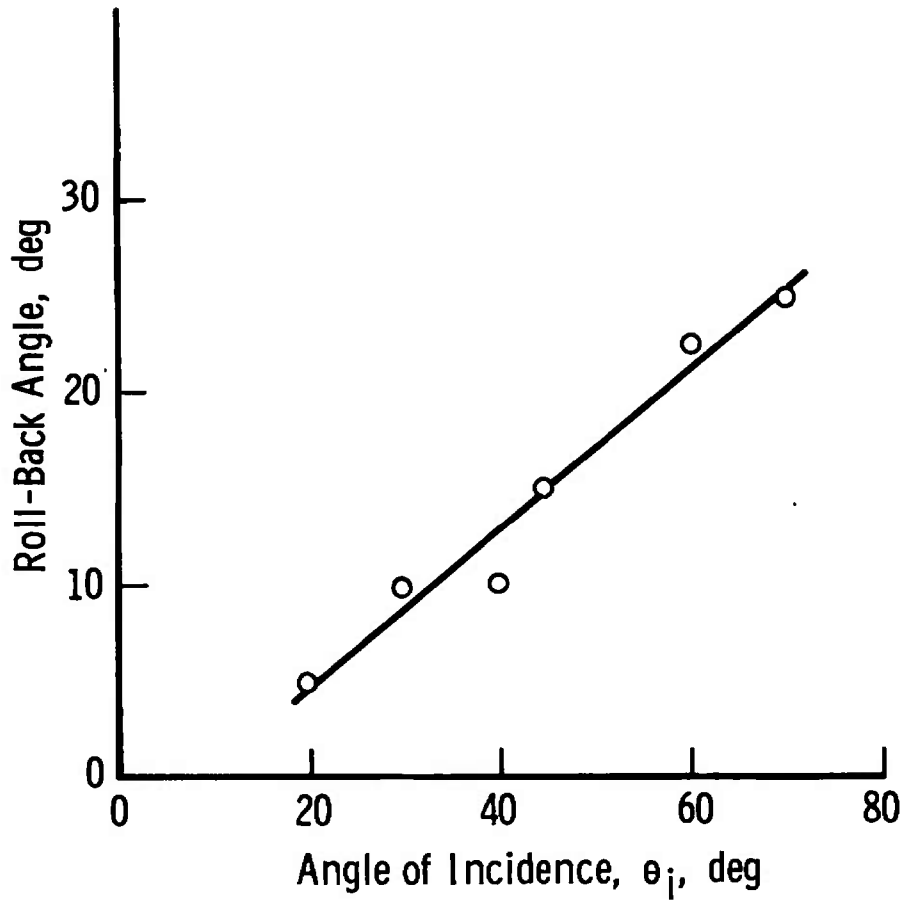

Fig. 11 Roll-Back Angle as a Function of Angle of Incidence, 300°K N_2 on a 300°K Vapor Blasted Aluminum Surface

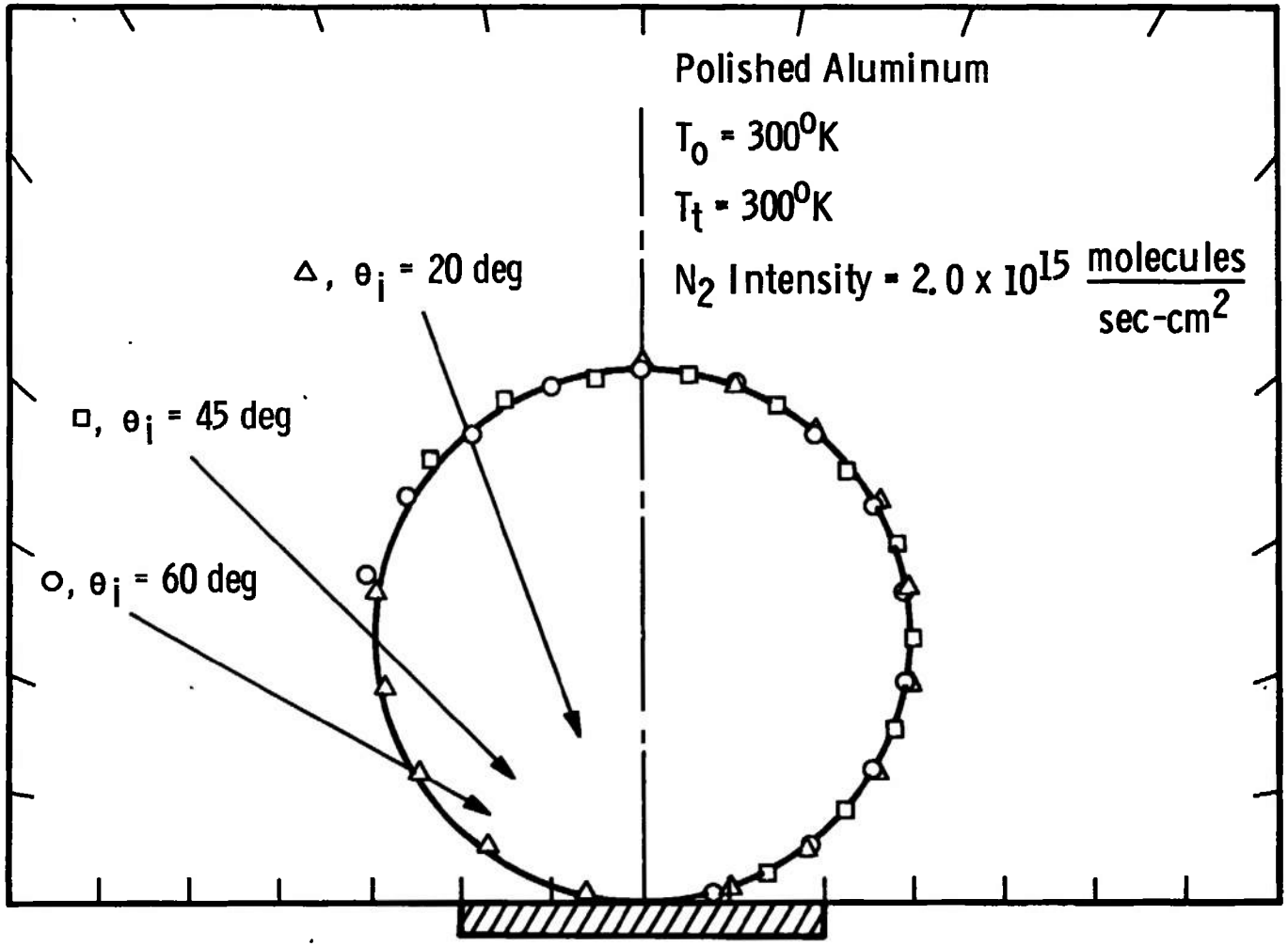

Fig. 12 Reflected Spatial Distribution of N_2 from a 300°K Polished Aluminum Surface for Various Incidence Angles

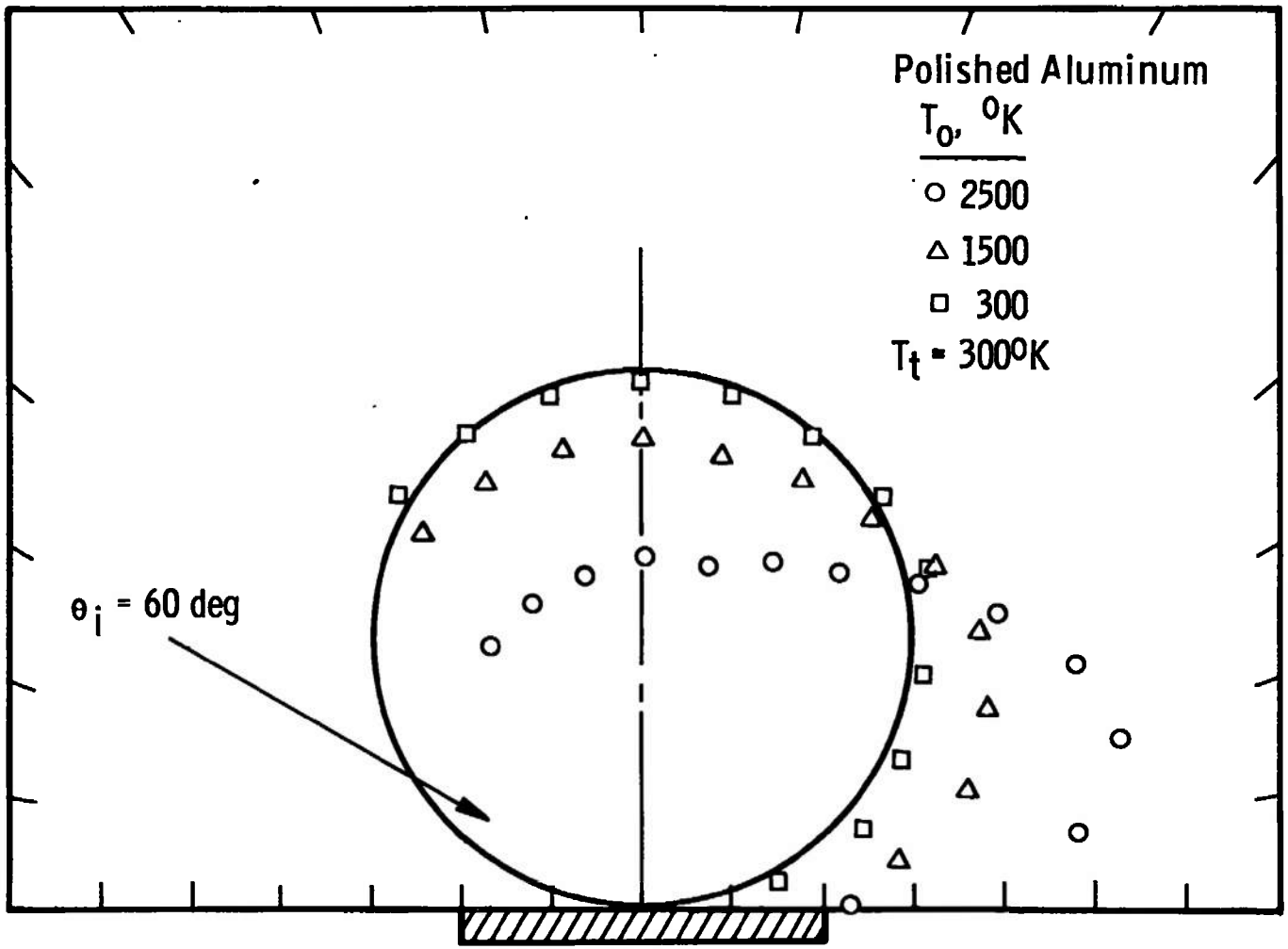

Fig. 13 Reflected Spatial Distribution of N_2 from a 300°K Polished Aluminum Surface for Various Incident Energies

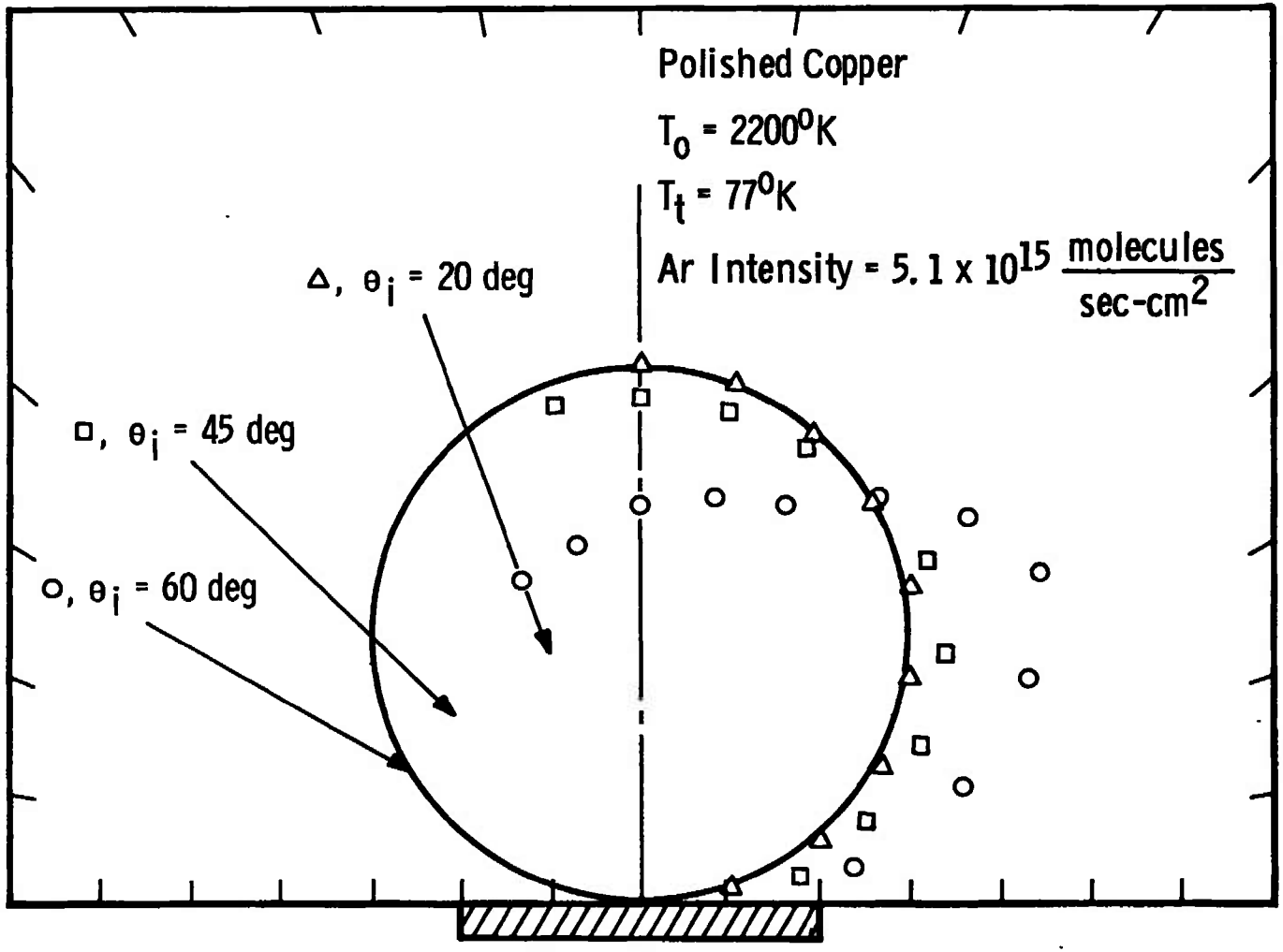

Fig. 14 Reflected Spatial Distribution of Argon from a 77°K Polished Copper Surface

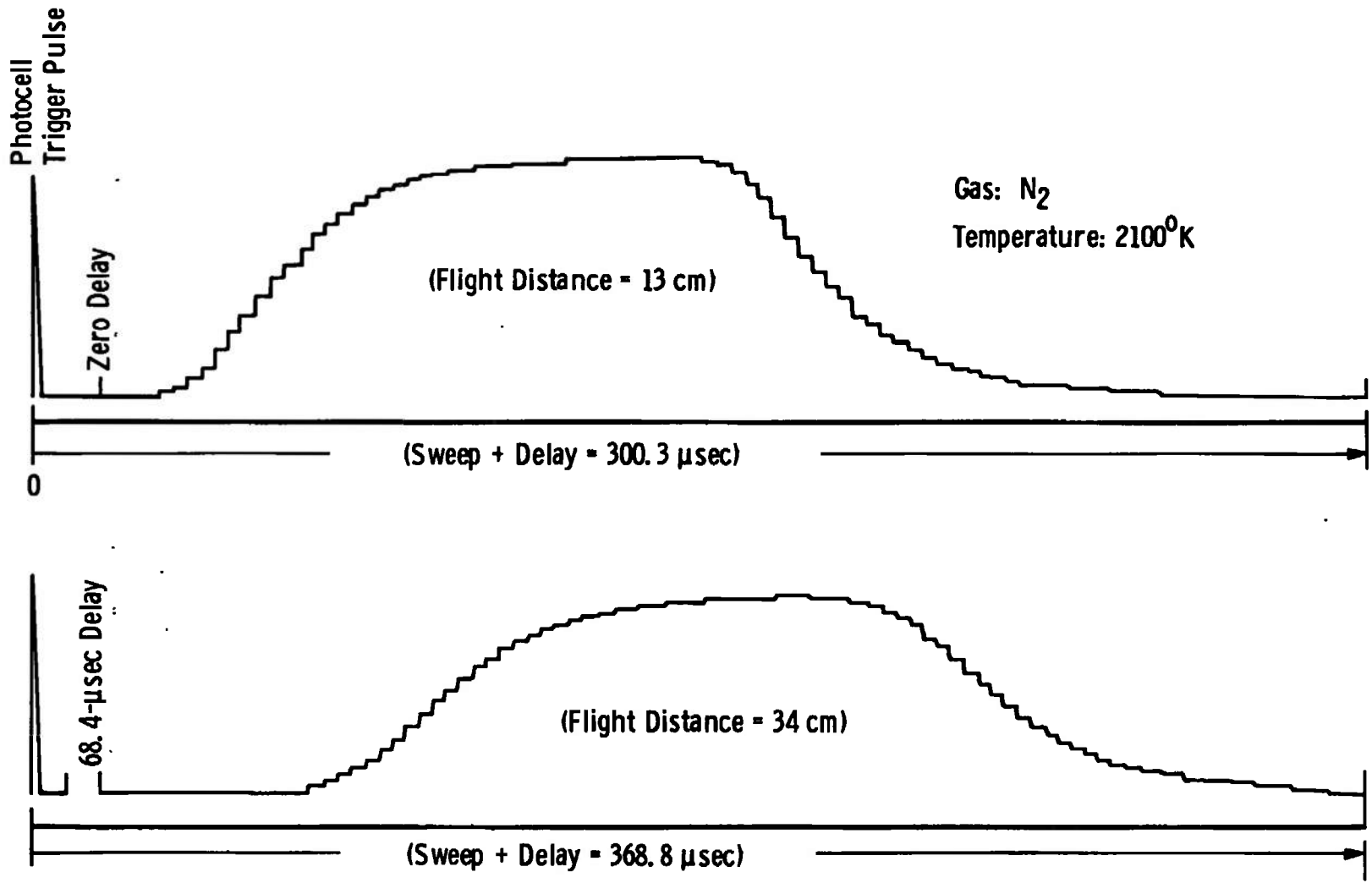

Fig. 15 Raw Signals Used to Determine Shutter Function

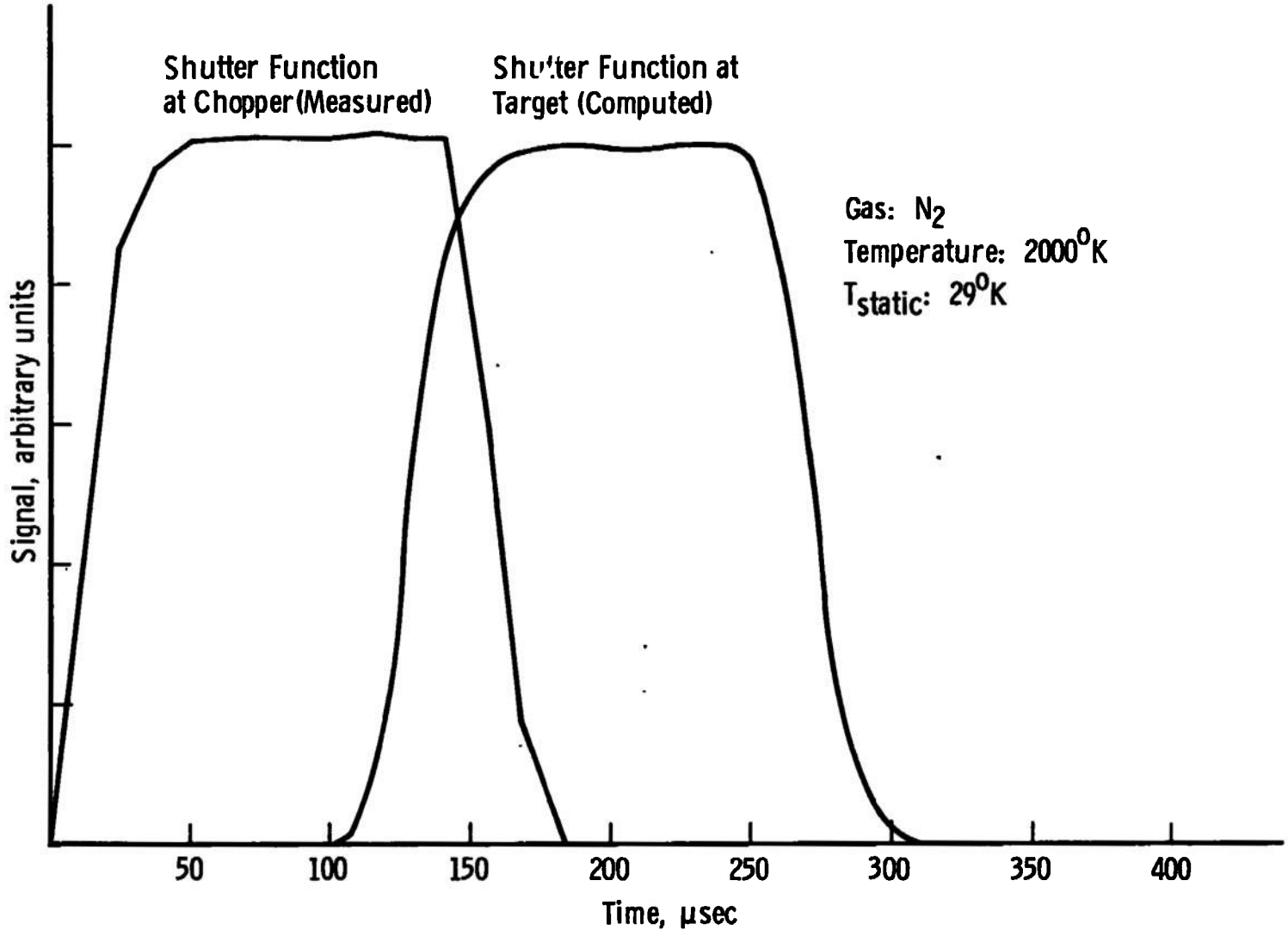

Fig. 16 Calculated Shutter Functions

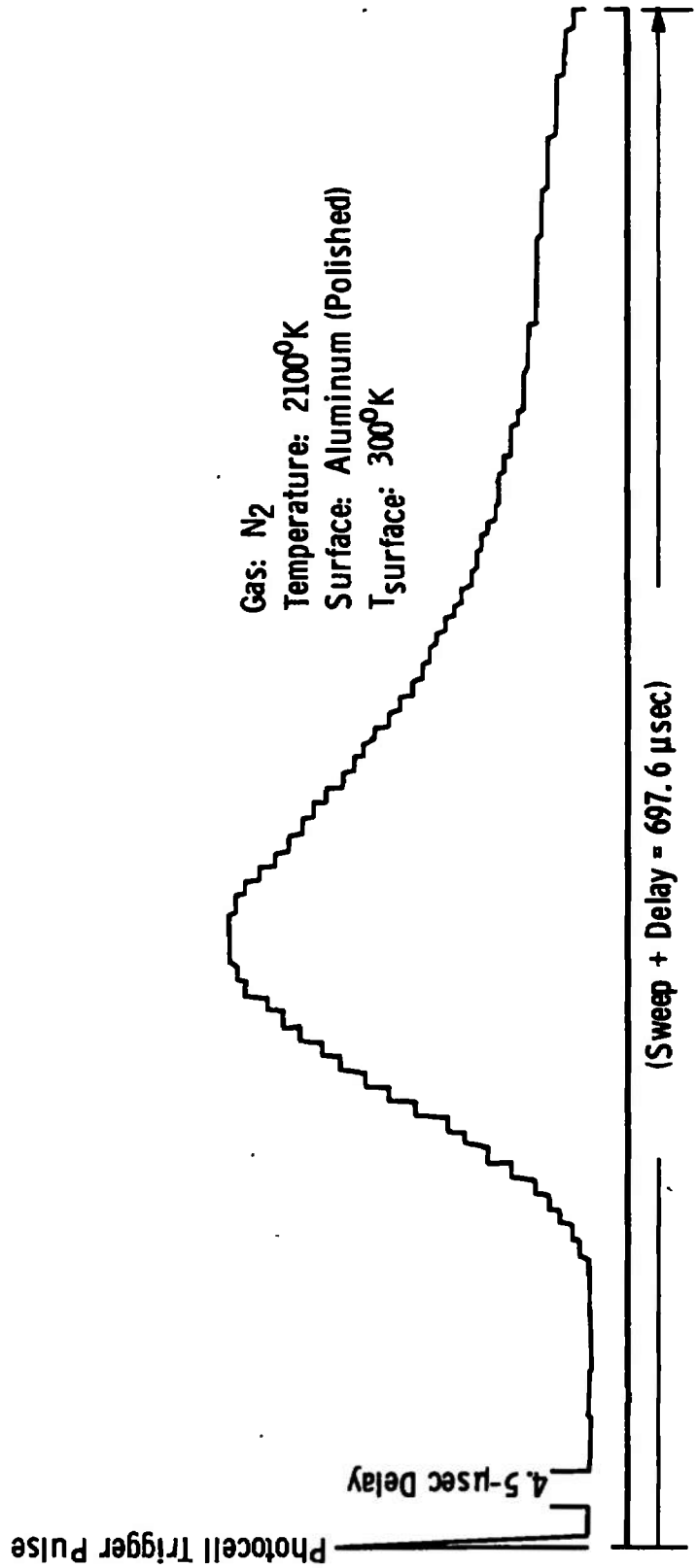

Fig. 17 Raw Signal from Reflected Molecular Pulse

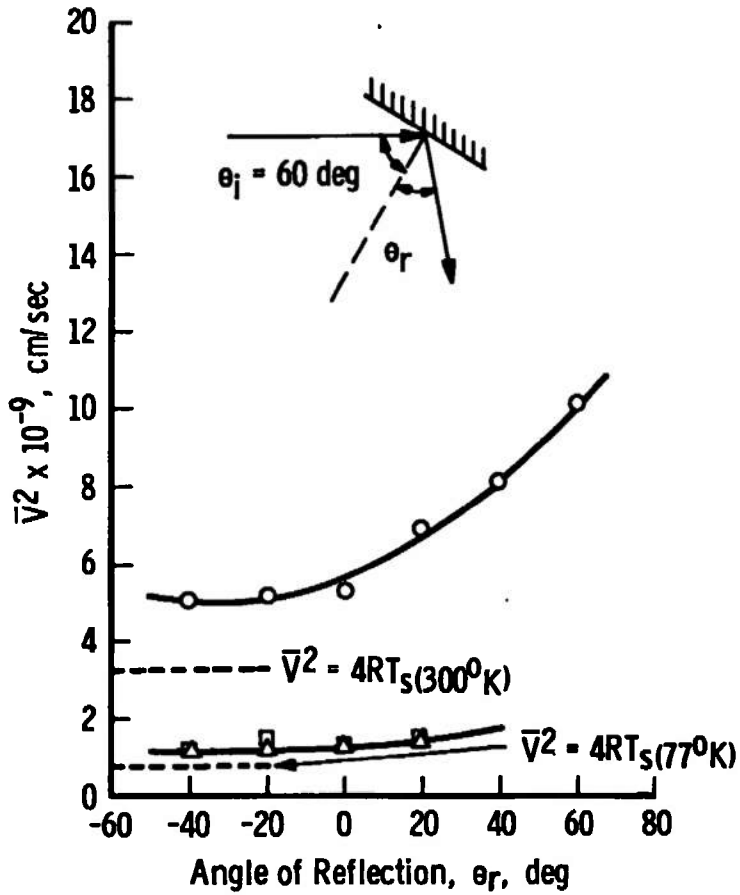

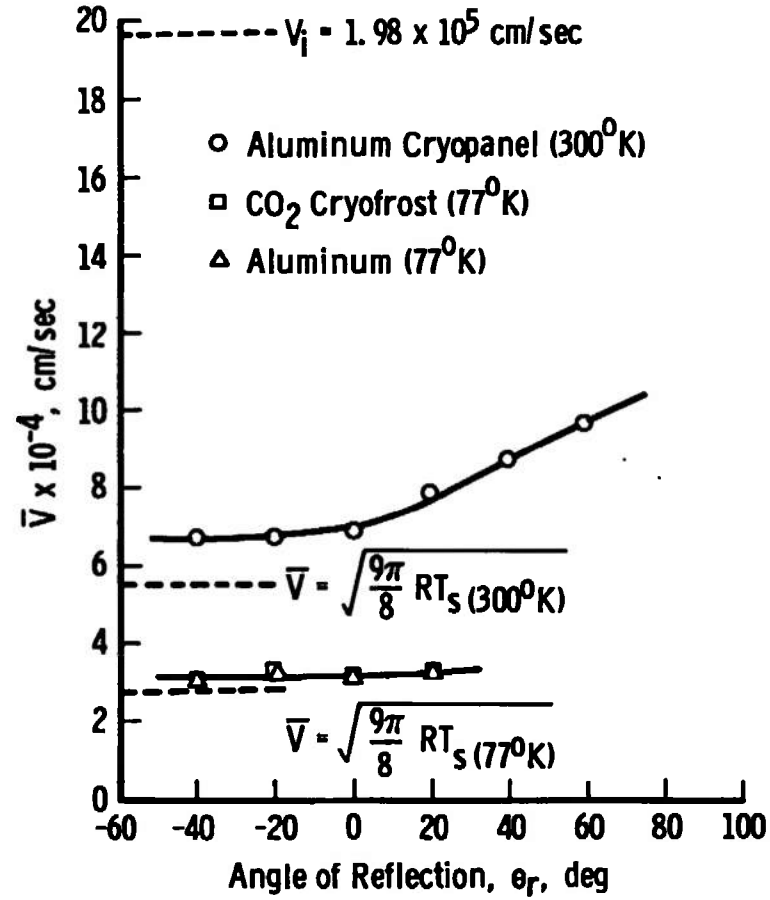

a. θ_i = 60 deg

Fig. 18 Reflected N_2 Velocity Distributions

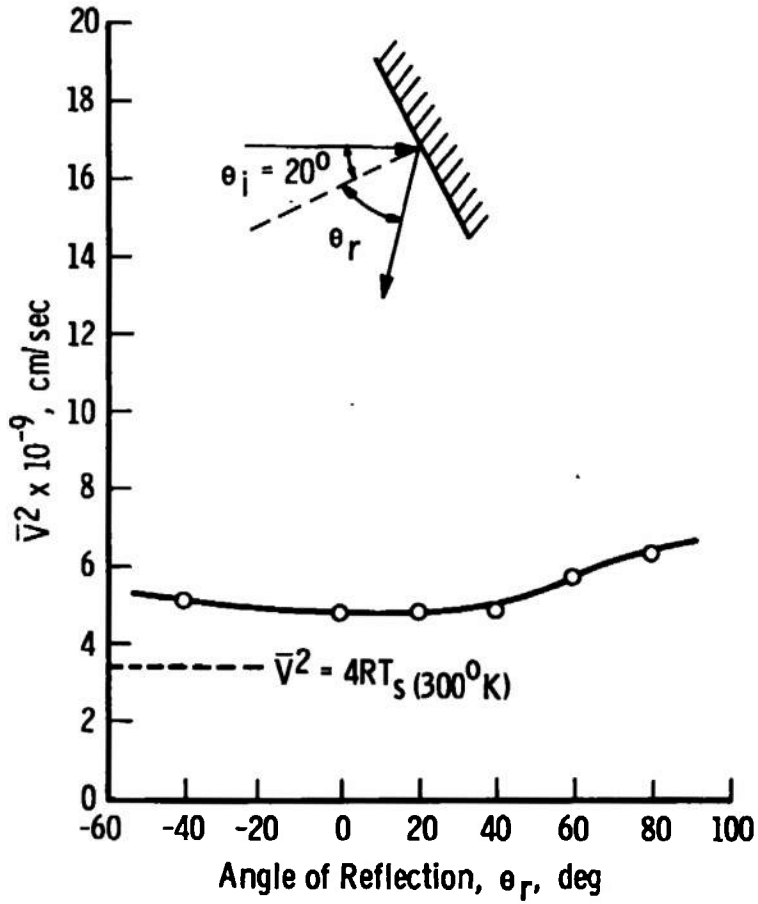

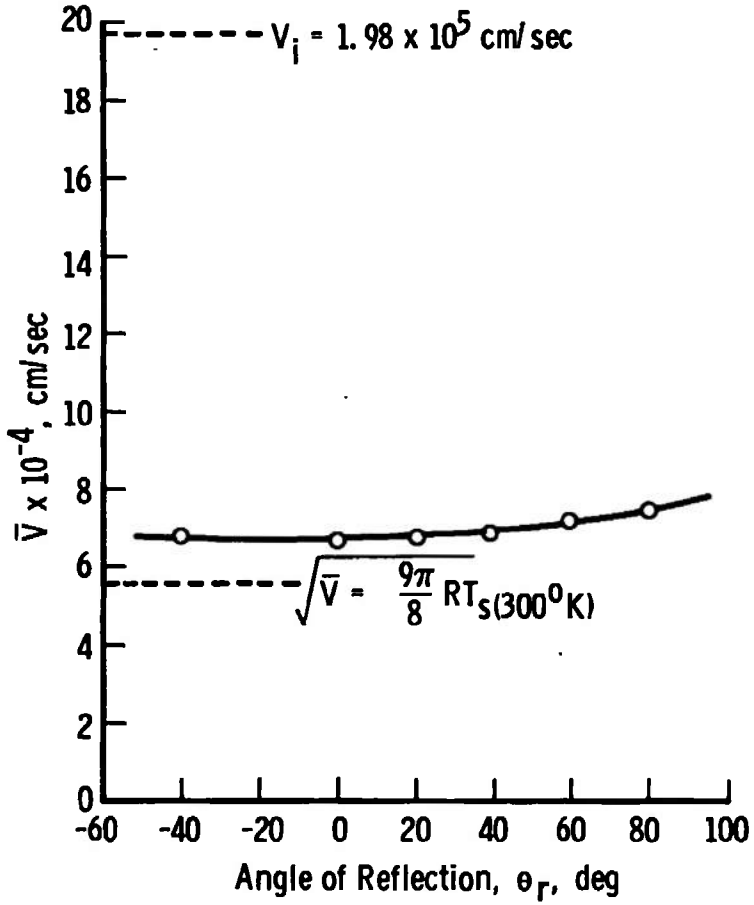

b. θ_i = 20 deg

Fig. 18 Concluded

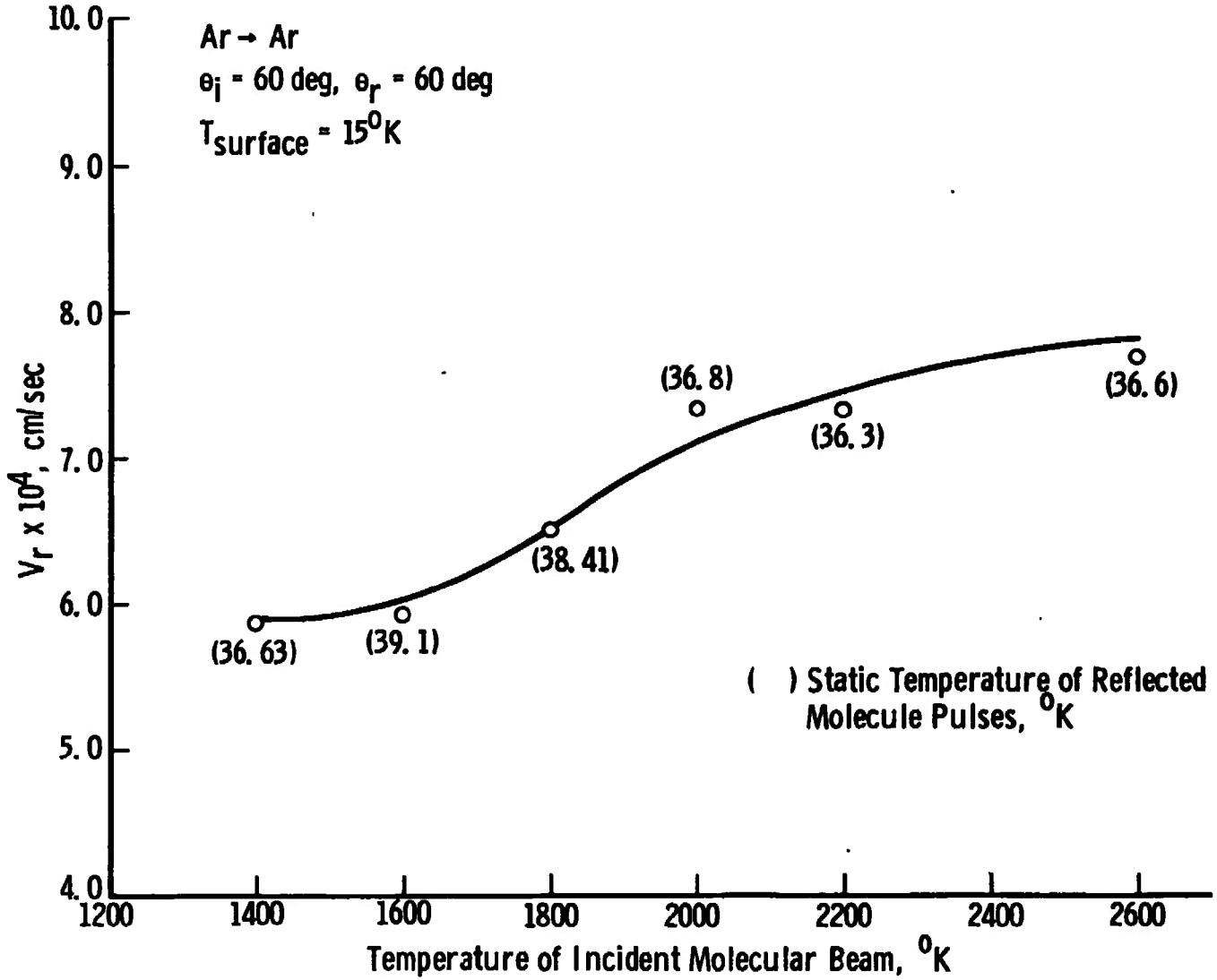

Fig. 19 Reflected Velocity of Argon from a 15°K Argon Cryodeposit

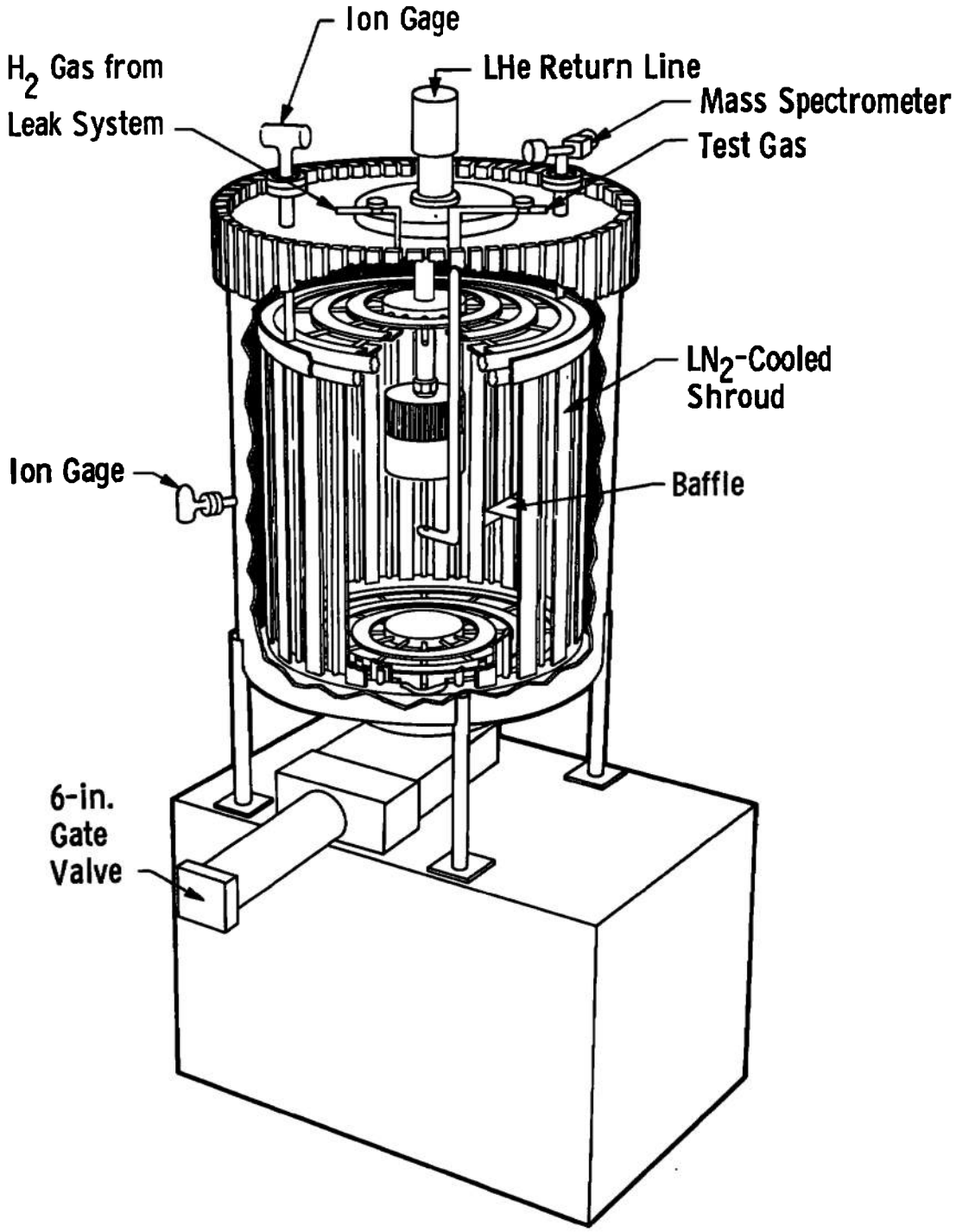

Fig. 20 2- by 3-ft Research Vacuum Chamber

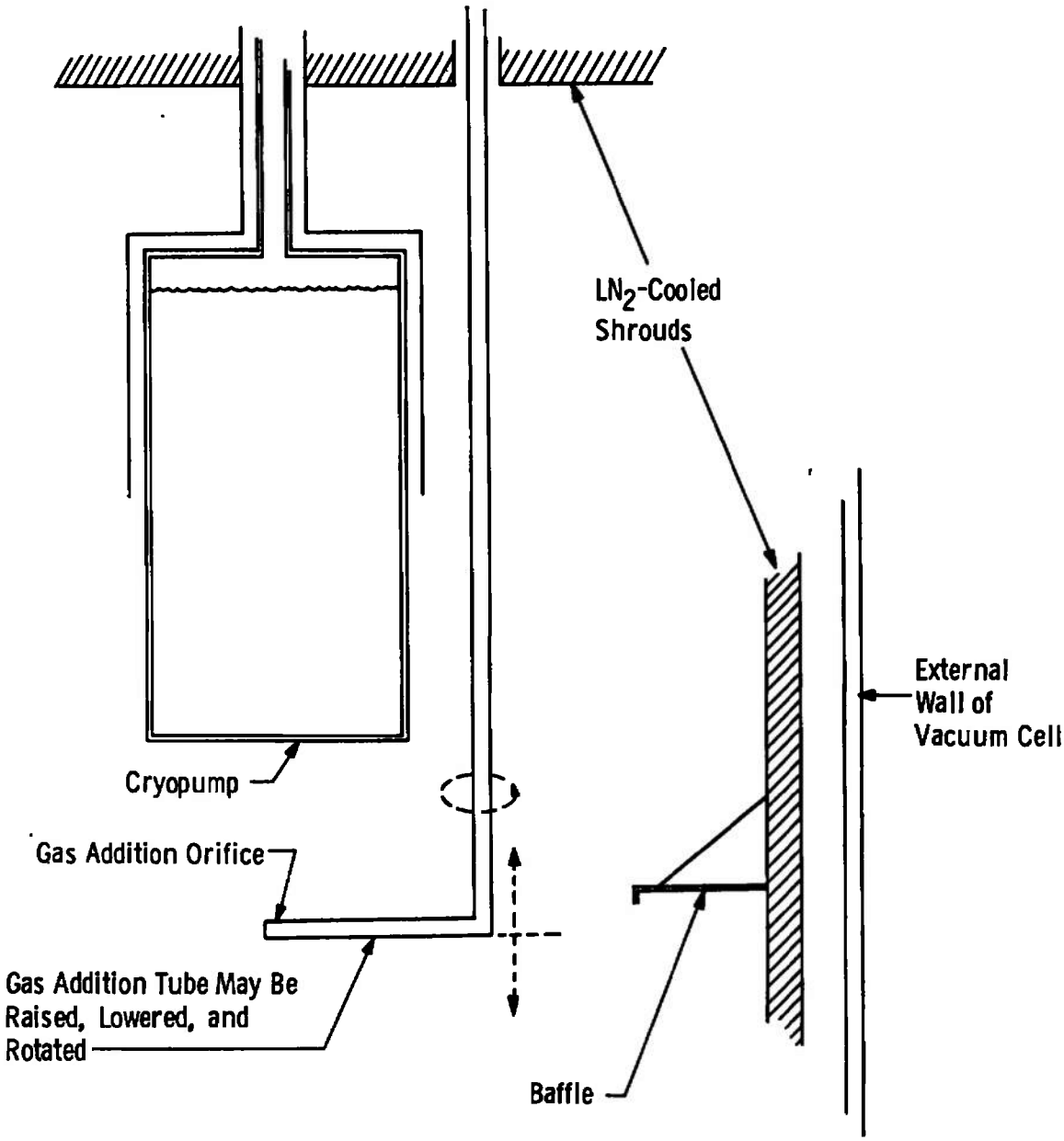

Fig. 21 Cryopump and Gas Addition Tube

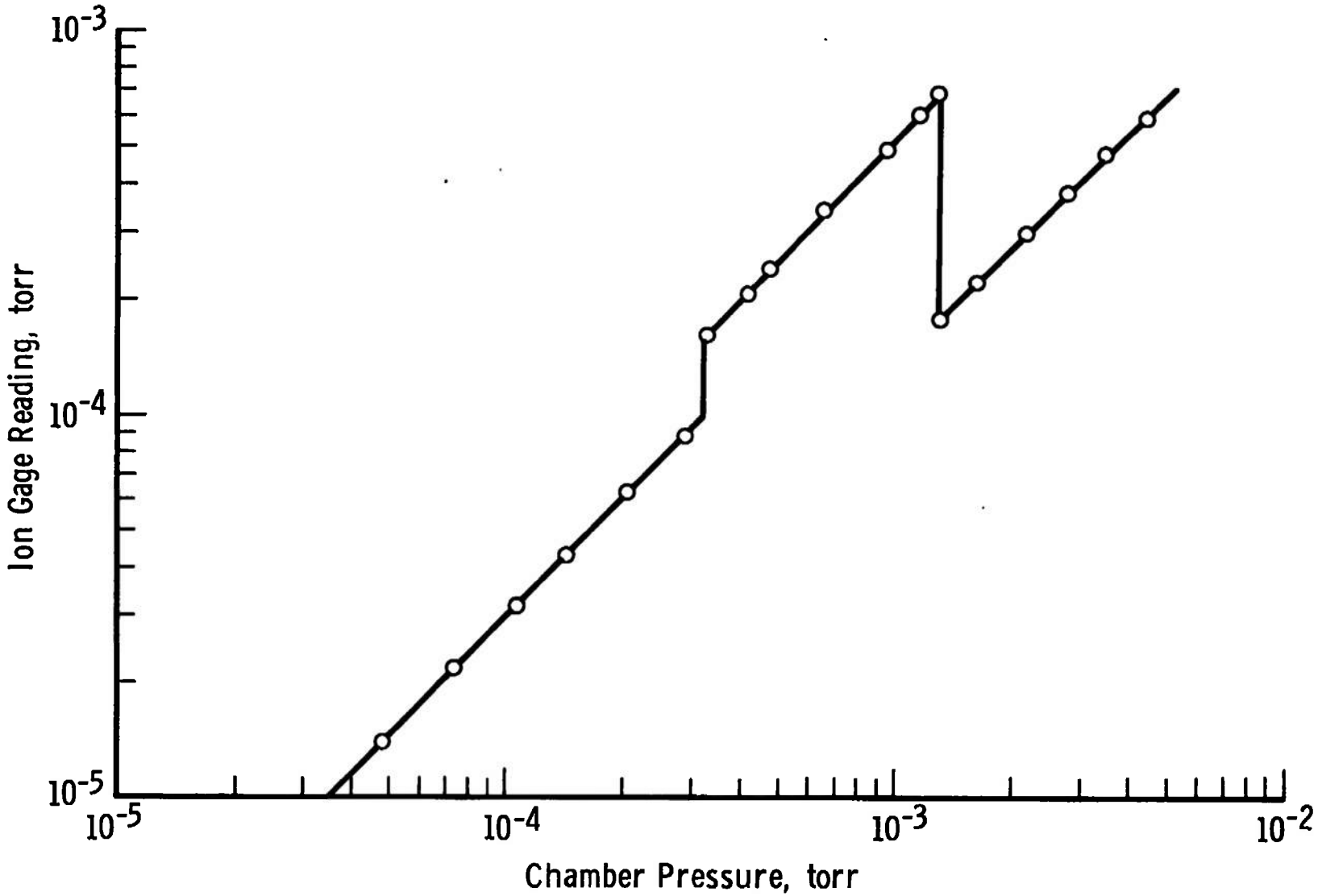

Fig. 22 Calibration Curve for Ion Gage

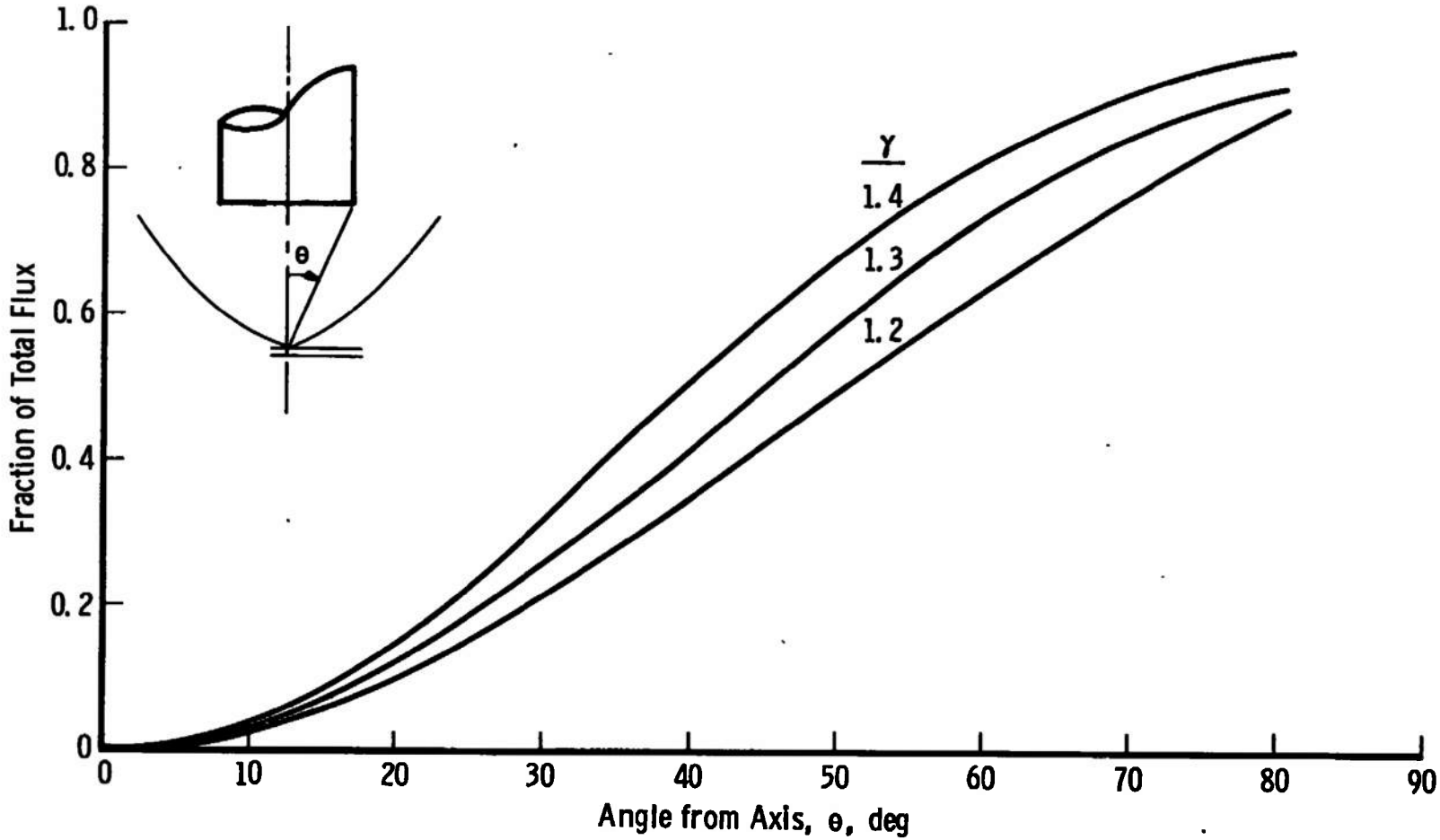

Fig. 23 Computer-Calculated Fraction of Mass Flow from a Sonic Orifice as a Function of Included Half-Angle

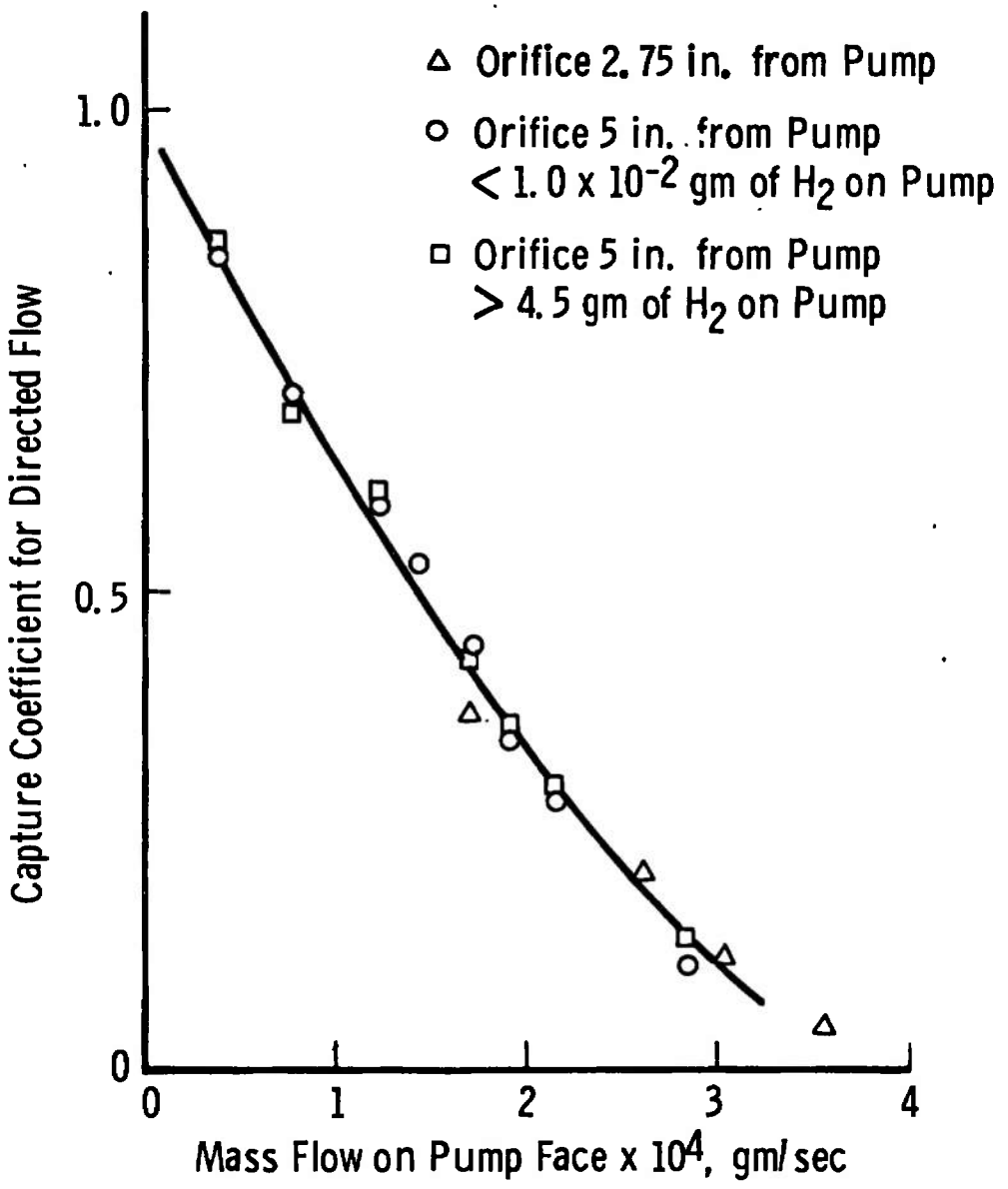

Fig. 24 Capture Coefficient on Cryosurface versus Mass Flow Rate Directly Incident

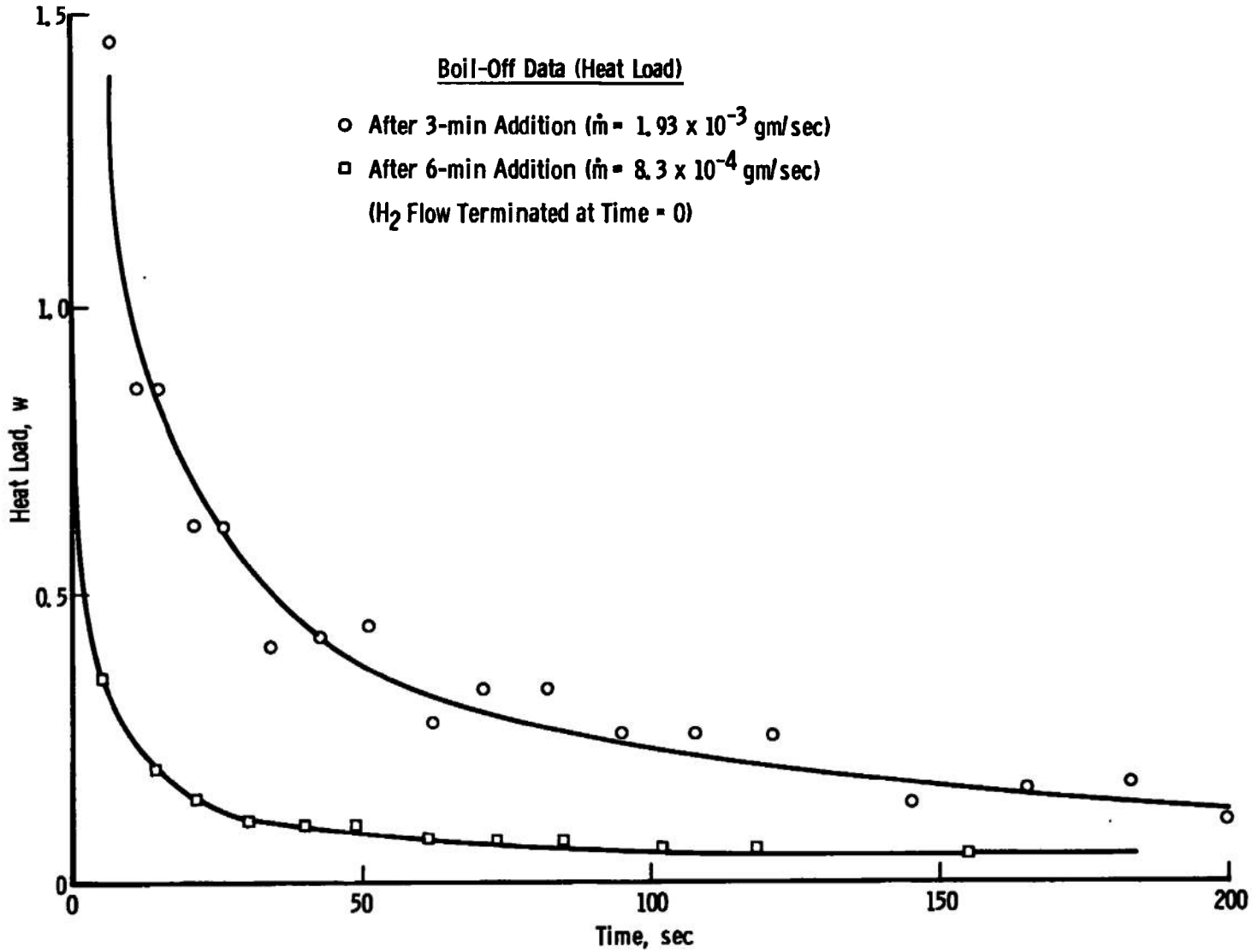

Fig. 25 Typical Heat Load Decay Curves

UNCLASSIFIED

Security Classification

DOCUMENT CONTROL DATA - R & D

(Security classification of title, body of abstract and indexing annotation must be entered when the overall report is classified)

1 ORIGINATING ACTIVITY *(Corporate author)*
Arnold Engineering Development Center,
Arnold Air Force Station, Tennessee 37389

2a. REPORT SECURITY CLASSIFICATION
UNCLASSIFIED

2b. GROUP
N/A

3 REPORT TITLE

STUDY OF HIGH-ENERGY GASES IMPINGING ON VARIOUS CRYOSURFACES

4. DESCRIPTIVE NOTES *(Type of report and inclusive dates)*
January 1970 to May 1971 - Final Report

5 AUTHOR(S) *(First name, middle initial, last name)*

R. Dawbarn, M. R. Busby and M. Kinslow, ARO, Inc.

6. REPORT DATE	7a. TOTAL NO OF PAGES	7b. NO. OF REFS
April 1972	57	12

8a. CONTRACT OR GRANT NO.	9a. ORIGINATOR'S REPORT NUMBER(S)
b. PROJECT NO.	AEDC-TR-72-33
c. Program Element 64719F	9b. OTHER REPORT NO(S) *(Any other numbers that may be assigned this report)*
d.	ARO-VKF-TR-72-3

10. DISTRIBUTION STATEMENT

Approved for public release; distribution unlimited.

11. SUPPLEMENTARY NOTES	12. SPONSORING MILITARY ACTIVITY
Available in DDC.	Arnold Engineering Development Center, AFSC, Arnold Air Force Station, Tennessee 37389

13. ABSTRACT A study of the interaction of high-energy molecular beams with various cryosurfaces was conducted in a molecular beam test facility. Spatial distributions of the reflected flux from several samples of typical engineering surfaces showed near-cosine distributions with some evidence of back scattering for roughened surfaces. For high-energy beams and highly polished surfaces there was a well-defined forward lobe of reflected molecules. Energy accommodation coefficients were determined by measuring the velocity of the reflected molecules. For all engineering surfaces tested the high-energy gases can be considered fully accommodated after one collision. Pumping studies of hydrogen (H_2) on liquid-helium (LHe)-cooled cryosurfaces were conducted. Capture coefficients close to 1.0 were measured for H_2 partial pressures up to 2×10^{-3} torr. For directed flows of H_2 on LHe-cooled panels there is an upper limit to the mass flow rate which will be cryopumped. This limit is determined by the thermal conductivity of the surface for stainless steel cryopanels and is apparently determined by cryofrost separation from the cryosurface for copper and aluminum cryopanels.

DD FORM 1 NOV 65 1473

UNCLASSIFIED

Security Classification

14. KEY WORDS	LINK A		LINK B		LINK C	
	ROLE	WT	ROLE	WT	ROLE	WT
cryogenics						
cryopumping						
molecular beams						
energy absorption						
reflection						
space environment simulation						